Prolonged White Matter Remodeling Trajectories Predict Cognitive and Emotional Recovery After Mild Traumatic Brain Injury

Aishwarya Rajesh

arajesh@wustl.edu

Washington University School of Medicine https://orcid.org/0000-0002-6583-1695

Timothy Laumann

https://orcid.org/0000-0002-0428-427X

Qing Wang

Washington University in St. Louis https://orcid.org/0000-0002-1296-7097

Meng Jiang

Washington University School of Medicine

Yong Wang

Washington University School of Medicine https://orcid.org/0000-0003-2507-8333

Deanna Barch

Washington University in St. Louis https://orcid.org/0000-0003-1693-8506

Benjamin Kay

Washington University School of Medicine https://orcid.org/0000-0003-3628-8029

Ashley Meyer

Washington University School of Medicine

Nico Dosenbach

Washington University School of Medicine https://orcid.org/0000-0002-6876-7078

Evan Gordon

Washington University School of Medicine https://orcid.org/0000-0002-2276-5237

Article

Keywords:

Posted Date: October 3rd, 2025

DOI: https://doi.org/10.21203/rs.3.rs-7682138/v1

Additional Declarations:
There is **NO** Competing Interest.

Supplementary Figures S1-S6 are not available with this version.

Prolonged White Matter Remodeling Trajectories Predict Cognitive and Emotional Recovery After Mild Traumatic Brain Injury

Aishwarya Rajesh[1], Timothy O. Laumann[2], Qing Wang[1], Meng Jiang[3], Yong Wang[1,3,4,5], Deanna Barch[1,2,6], Benjamin P. Kay[7], Ashley C. Meyer[1], Nico U.F. Dosenbach[1,5,7-10], Evan M. Gordon[1]

Departments of [1]Radiology, [2]Psychiatry, [3]Obstetrics and Gynecology, [4]Electrical and System Engineering, [5]Biomedical Engineering, [6]Psychological and Brain Sciences, [7]Neurology, [8]Neuroscience, [9]Pediatrics, and [10]Program in Occupational Therapy, Washington University in St. Louis, MO

Abstract

Traumatic brain injury (TBI) disrupts white matter tracts essential for cognition and emotion. Although diffusion tensor imaging (DTI) can noninvasively measure white matter structure, it has been inconsistent in predicting recovery from TBI, likely due to complex, individual-specific dynamics of post-TBI white matter remodeling. Here, we employed dense longitudinal neuroimaging to track white matter recovery weekly over six months after complicated mild TBI in a single 21 y.o. patient (motor vehicle collision; Glasgow Coma Score = 15; no loss of consciousness or post-traumatic amnesia; visible right temporal subdural hematoma) and a 24 y.o. control. Across both individuals, we collected 56 MRI sessions totaling over 2,500 minutes of high-quality scanning and matched behavioral assessments, offering an exceptionally dense view of within-participant white matter remodeling. In the patient, but not the control, fractional anisotropy (FA)—a widely used DTI metric—showed sustained decreases across many tracts before reversing course around 18 weeks post-injury, suggesting nonlinear and prolonged reorganization. These continuous changes in FA also mediated improvements in cognitive and emotional function, implying that FA reflects active recovery processes, not just damage. Diffusion basis spectrum imaging (DBSI) revealed an initial phase of cellular loss, followed by inflammatory remodeling, vascular adaptation, and persistent metabolic activity. These brain changes lasted over six months, far exceeding the few days of cognitive rest typically recommended in clinical care. These findings challenge current return-to-activity guidelines and suggest the possibility of tailoring rehabilitation timing to individual patterns of brain recovery, rather than relying on broad, standardized recovery windows.

Introduction

Nearly half of the global population is expected to experience a traumatic brain injury (TBI) in their lifetime (Jiang et al., 2023; Maas et al., 2022). In TBI, shearing forces during head impact disrupt the microstructural integrity of white matter tracts (Gennarelli et al., 1982). These tracts connect distant brain regions that support cognition and behavior (Schmahmann et al., 2008, Filley 2012, Catani et al., 2012, Forkel et al., 2021, Roberts, Anderson, & Husain, 2013). Perhaps as a result, TBI is commonly accompanied by deficits in cognitive and/or emotional function (Filley & Kelly, 2018, Spitz et al., 2017, Hellstrøm et al., 2017).

TBI is a dynamic rather than a static condition, as it involves an extended post-injury recovery period during which impaired cognitive and emotional processes generally improve (Caroll et al., 2004; Shretlen & Shapiro, 2003; Frencham, Fox, & Maybery, 2005). The post-TBI recovery period can be conceptualized as the interval beginning after acute stabilization and extending through subacute and chronic phases of recovery, during which white matter is remodeled and (where possible) repaired, and brain function gradually improves. However, there is little consensus on precise time boundaries, with studies defining subacute recovery as anywhere from one week to three months post-injury and chronic recovery extending beyond three months (Amyot et al., 2015; Wallace, Mathias, & Ward, 2018).

Despite this lack of consensus on recovery timing, clinical guidance for recovery remains largely based on symptom resolution, and the mainstay of treatment—rest—is often prescribed without objective biological markers to guide its duration (Silverberg & Iverson, 2013; McCrory et al., 2008; Weil, Ivey, & Karelina, 2023). Standard recommendations advise temporary withdrawal from work, school, and sports to reduce the risk of reinjury and allow the brain to heal (Silverberg & Iverson, 2013; Lumba-Brown et al., 2018). This guidance often takes the form of the widely adopted “rest until asymptomatic” approach, which, while intuitive, may not align with the brain’s true physiological recovery timeline (Alla, Sullivan, & McCrory, 2012). In fact, many clinicians encourage patients to resume daily activities within a few days after injury (Thomas et al., 2015). Yet this practice may be ill-advised: premature return to activity could occur during a period of ongoing biological vulnerability, increasing the risk for reinjury or prolonged recovery (Griesbach et al., 2012; Silverberg & Iverson, 2013). Evidence-based guidance about when recovery is complete, and when return-to-activity can safely and fully resume, remains elusive, in large part because few studies have captured the evolving biological processes that unfold during recovery.

White matter damage induced by TBI is best assessed noninvasively using diffusion tensor imaging (DTI), a neuroimaging technique that measures the movement of water molecules in the brain (Hulkower et al., 2013). In healthy white matter, water diffusion is anisotropic (directionally constrained), occurring primarily along axonal pathways due to the restrictive influence of myelin sheaths and cellular structures.

When these tracts are disrupted, water diffusion becomes more isotropic (equal in all directions). Fractional anisotropy (FA), the most commonly used DTI metric, indexes the degree of directionality in water diffusion. FA is consistently reduced in individuals who have experienced a TBI compared to healthy controls (Mac Donald et al., 2011, Nakayama et al., 2006; Hulkower et al., 2013; Niogi & Pratik, 2010), reflecting a shift toward more isotropic diffusion and suggesting greater white matter disruption.

Ideally, DTI metrics would provide mechanistic and clinically predictive power for tracking the recovery process and informing return-to-activity decisions. Yet while DTI metrics consistently differ between individuals with and without TBI, their relationship with recovery remains unclear. Prior work has shown FA to increase (Chiou et al., 2019; Ling et al., 2012; Mayer, 2010), decrease (Niogi & Pratik, 2010; Veeramuthu et al., 2016; Næss-Schmidt et al., 2017; Karlsen et al., 2019; Palacios et al., 2020), or remain unchanged (Eirud et al., 2014; Narayana et al., 2015; Wilde et al., 2016) during the recovery period (Kim et al., 2022). Similarly, although DTI alterations are cross-sectionally associated with cognitive deficits (Preziosa et al., 2022; Gyebnár et al., 2018; Mesaros et al., 2012; Brickman et al., 2006) and mood symptoms (Sexton, Mackay, & Ebmeier, 2009; Murphy & Frodl, 2011; Catani et al., 2012; Zhang et al., 2011; Han et al., 2008), it remains unclear whether recovery from these deficits is supported by longitudinal changes in DTI metrics.

Study design limitations have played a role in preventing DTI from becoming a reliable tool for tracking TBI recovery in clinical settings. First, most DTI studies tracking post-TBI recovery collect only two to three post-injury timepoints (Kim et al., 2022). This sparse sampling limits the ability to track the dynamics of white matter changes over the course of recovery or to establish associations with the resolution of cognitive and emotional symptoms. Second, most DTI studies rely on group-level designs that average across patients and brain regions. This approach overlooks the substantial heterogeneity in brain anatomy, injury characteristics and recovery trajectories (Rosenbaum & Lipton, 2012, Kim et al., 2022; Eirud et al., 2014). As a result, such studies lack the precision needed to capture meaningful recovery-related changes and thus may not directly inform mechanisms of within-individual TBI recovery, which in turn poses challenges for developing clinically relevant neuroimaging approaches. In contrast, detailed and extensive longitudinal data from an individual could offer a clearer view of within-person recovery dynamics, potentially revealing patterns obscured by group averaging.

Recently, an approach termed precision imaging has emerged as a powerful alternative to traditional group-based neuroimaging (Gordon et al., 2017). By leveraging dense, repeated scanning of individuals, precision imaging maximizes the reliability of neuroimaging measures that are often affected by noise and inter-individual variability (Laumann et al., 2015; Gordon et al., 2023; Gratton, Nelson, & Gordon, 2022; Braga & Buckner, 2017; Naselaris et al., 2021; Michon et al., 2022). Single-participant designs

have enabled insights into dynamic brain processes such as mood variability (Lynch et al., 2024), motor learning (Newbold et al., 2020), and hormonal rhythms across the menstrual cycle (Pritschet et al., 2020) and pregnancy (Pritschet et al., 2024). These studies illustrate the unique value of individualized approaches for capturing fine-grained biological change. In clinical contexts like TBI, where recovery trajectories are highly individualized, precision imaging may be particularly valuable for characterizing how brain structure and function evolve over time.

To this end, we used a densely sampled, longitudinal precision imaging approach to track individual-level white matter changes following a case of complicated mild TBI in a 21-year-old female who sustained a right temporal subdural hematoma (SDH, 11×8 mm) from a motor vehicle collision. She presented to the emergency department with a Glasgow Coma Scale score of 15, reported headache but no neurological deficits, and had no loss of consciousness (LOC) or post-traumatic amnesia (PTA). An age-matched healthy control (24-year-old male) with no history of neurological or psychiatric conditions was also scanned. Both participants completed 28 MRI sessions and behavioral assessments, including weekly for 27 weeks beginning two weeks post-injury (or post enrollment, for the control participant), plus a one-year follow-up. Each session included 45 minutes of high-resolution neuroimaging, totaling over 2,500 minutes of MRI data and 56 behavioral assessments across both participants, providing a uniquely dense view of post-injury recovery dynamics.

Importantly, DTI metrics like FA reflect not only the degree of intact anisotropic diffusion, but also dynamic secondary injury processes such as inflammation, edema, and axonal repair (Armstrong et al., 2016, Palacios et al., 2020). Yet, it remains unclear which of these processes most closely relate to post-TBI symptomatic improvement. To resolve this ambiguity, we further employed Diffusion Basis Spectrum Imaging (Wang et al., 2019a, 2015, 2011), an advanced technique that can disentangle these overlapping processes to improve biological specificity in characterizing TBI-related white matter changes. Together, the dense, repeated imaging collected for this study enables an unprecedented, integrated analysis of white matter recovery trajectories and their association with behavioral outcomes. It represents a critical step forward in defining how white matter integrity evolves post-TBI and in laying the groundwork for biomarker-driven, individualized rehabilitation strategies.

Results

Nonlinear white matter trajectories reveal dynamic post-TBI remodeling

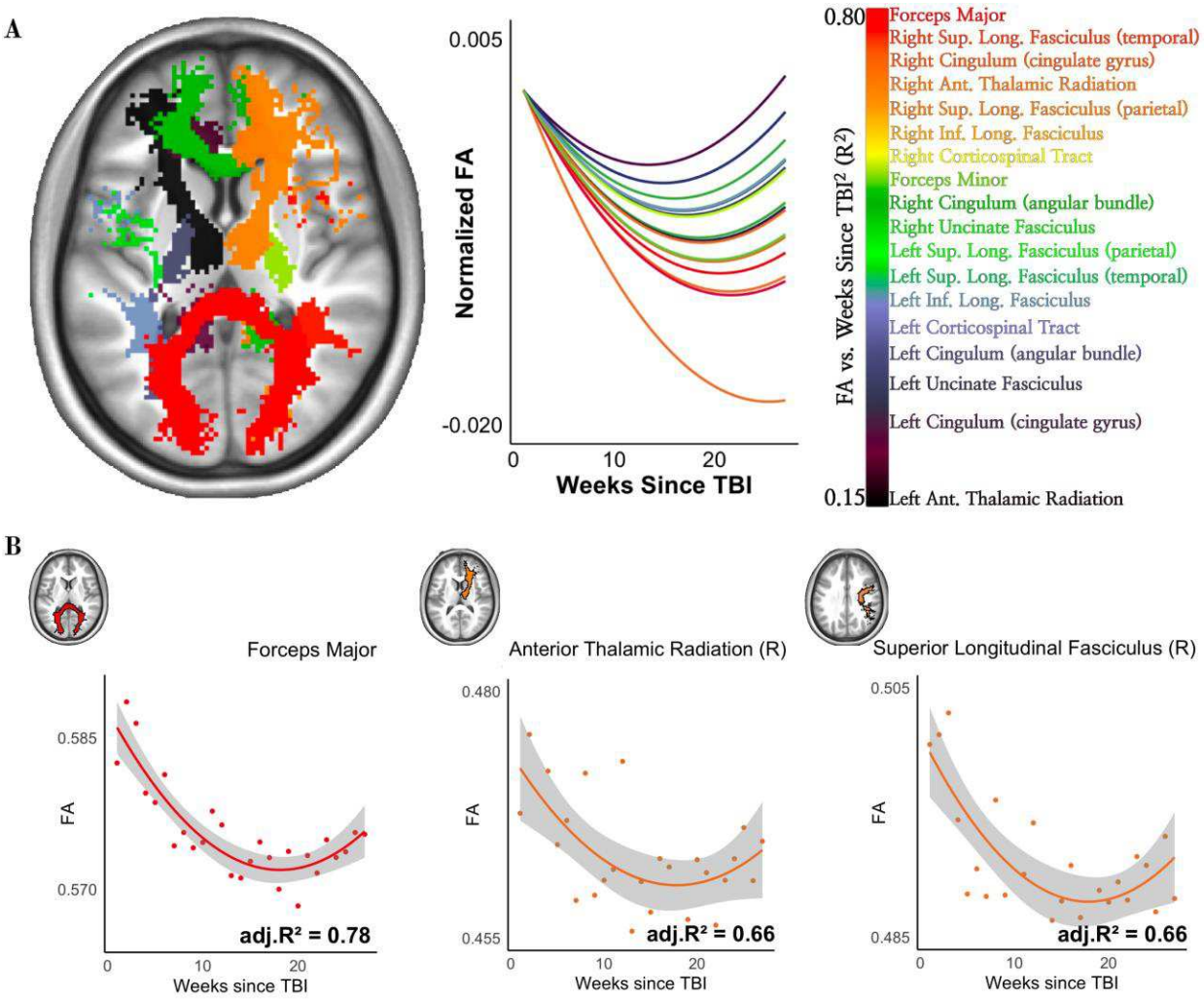

Figure 1: Nonlinear Trajectories of Fractional Anisotropy Changes (FA) Over Time Post-TBI. (A) Left: White matter tracts in the TBI patient are colored by strength of model (quadratic) fit for FA over time (in weeks) since TBI. Tracts in orange-red indicate a strong relationship (variance explained ~80%), while tracts in purple-black indicate a weaker relationship (variance explained ~15%). Right: FA trajectories across all 18 tracts over time, based on the best-fitting quadratic model with random slope effects. FA trajectories are normalized by each tract's predicted Week 1 value to enable simultaneous visualization of all tracts. FA declines more rapidly in the early weeks post-injury before reversing direction, rather than following a simple linear trajectory. (B) FA trajectories over time in three example tracts: forceps major (commissural tract), right anterior thalamic radiation (projection tract), and right superior longitudinal fasciculus (association tract).

In both a complicated mild TBI patient (21F, right temporal SDH, GCS 15, no LOC/PTA) and a control participant (24M, no history of neurological or psychiatric conditions), 18 major white matter tracts were defined using TRACULA (Yendiki et al., 2011). DTI metrics including fractional anisotropy (FA), radial diffusivity (RD), axial diffusivity (AD), and mean diffusivity (MD) were extracted from each of these tracts for each neuroimaging session.

Because prior studies have typically modeled FA and other DTI metrics as changing linearly over time (Kim et al., 2022), we began by testing linear models. However, given the possibility that white matter recovery may involve a return of DTI metrics toward pre-injury levels, we also tested quadratic models. Mixed-effects modeling showed that quadratic models fit the data substantially better than linear models for FA, RD, and MD (ps < 10^{-8}, ΔAIC > 10; see Table 1). Visual inspection revealed a consistent pattern across tracts in the TBI patient: FA declined during the early weeks post-injury, then gradually stabilized and began to increase, consistent with a recovery trajectory (Figure 1A–B). RD and MD showed the opposite pattern, increasing early on and then gradually declining (Fig. S1A–B, E–F). In contrast, AD exhibited a more linear, steadily increasing trajectory (Fig. S1C–D).

The quadratic models explained a substantial proportion of variance in each measure over the course of recovery. Across tracts, variance explained averaged ~50% for FA (Fig 1A, S2) and RD (Fig S1A, B), and 30% for MD (Fig S1E, F), with particularly strong fits in tracts like the forceps major (Fig 1B, S1B, S1F). AD was best explained by a linear model, though the variance explained was substantially weaker (~10%; Fig. S1C, D). 10 out of 18 tracts showed a significant relationship between FA and weeks since TBI^2, 9 out of 18 tracts showed a significant relationship for RD, and 4 out of 18 tracts showed a significant relationship for MD. Although AD changes were statistically detectable across 6 out of 18 tracts for weeks since TBI, the variance explained was relatively low, reflecting small but consistent effects.

In contrast, the control participant showed only minimal changes over time. Although quadratic models still fit better than linear ones (Table 1)—they explained very little variance—averaging 6% for FA, 3% for RD, and 7% for MD (Fig. S3). AD was again best fit by a linear model, with only ~2% variance explained. No tracts showed significant relationships with weeks since TBI^2 for any metric. Together, these findings suggest that white matter changes in the TBI patient reflect remodeling processes across time that are not present in the uninjured control.

Table 1: Model Selection across White Matter Metrics in the TBI Patient

Metric	ΔAIC (L-Q)	ANOVA (p-value)	Selected Model	Random Effect	$R^2_{marginal}$ %	$R^2_{conditional}$ %
FA	53.3	1×10^{-13} (***)	Q	Slope	0.5	99.2
RD	62	2×10^{-15} (***)	Q	Slope	0.5	99.5
AD	0	0.3	L	Intercept	0.1	99.3
MD	32	7×10^{-9} (***)	Q	Intercept	0.3	99.3
Fiber	62	1×10^{-15} (***)	Q	Slope	2.0	70.0
Cellularity	67	$<2\times10^{-16}$ (***)	Q	Slope	1.5	94.9
Free Water	100	$<2\times10^{-16}$ (***)	Q	Slope	1.4	81.1
Hindered	-1	0.3	L	Intercept	0.5	89.8
Perfusion	-1	0.3	L	Intercept	4.0	51.2

Table 1: Model selection results for white matter metrics in the TBI patient, comparing linear (L) and quadratic (Q) models using the Akaike Information Criterion (AIC) and ANOVA-based significance testing favoring quadratic models ($p < 0.001$ ***). ΔAIC (L-Q) represents the difference between linear and quadratic models (values >10 favor quadratic models; Burnham & Anderson, 2002). Model selection followed a two-step process: (1). *Model Stability Assessment*: Each model was tested across 1000 bootstrapped simulations to check for convergence and avoid boundary fit issues. (2). *Random Effects Evaluation*: The inclusion of random effects was tested by comparing models with and without them using ANOVA, to determine whether a simpler model without random effects provided a better fit. If a model failed across any simulation or the random effect was non-significant, the model was simplified stepwise (Barr et al., 2013): Quadratic model with random slope → Quadratic model with random intercept → Linear model with random slope → Linear model with random intercept → Simple linear regression (if necessary). The "Selected Model" column shows the best-fitting model, and "Random Effect" indicates whether a slope or intercept was retained as a random effect. $R^2_{marginal}$ represents the proportion of variance explained only by the fixed effects (i.e., Weeks Since TBI, Head Motion, and for quadratic models, Weeks Since TBI^2). $R^2_{conditional}$ represents the total variance explained by both fixed and random effects, incorporating variability due to individual tracts.

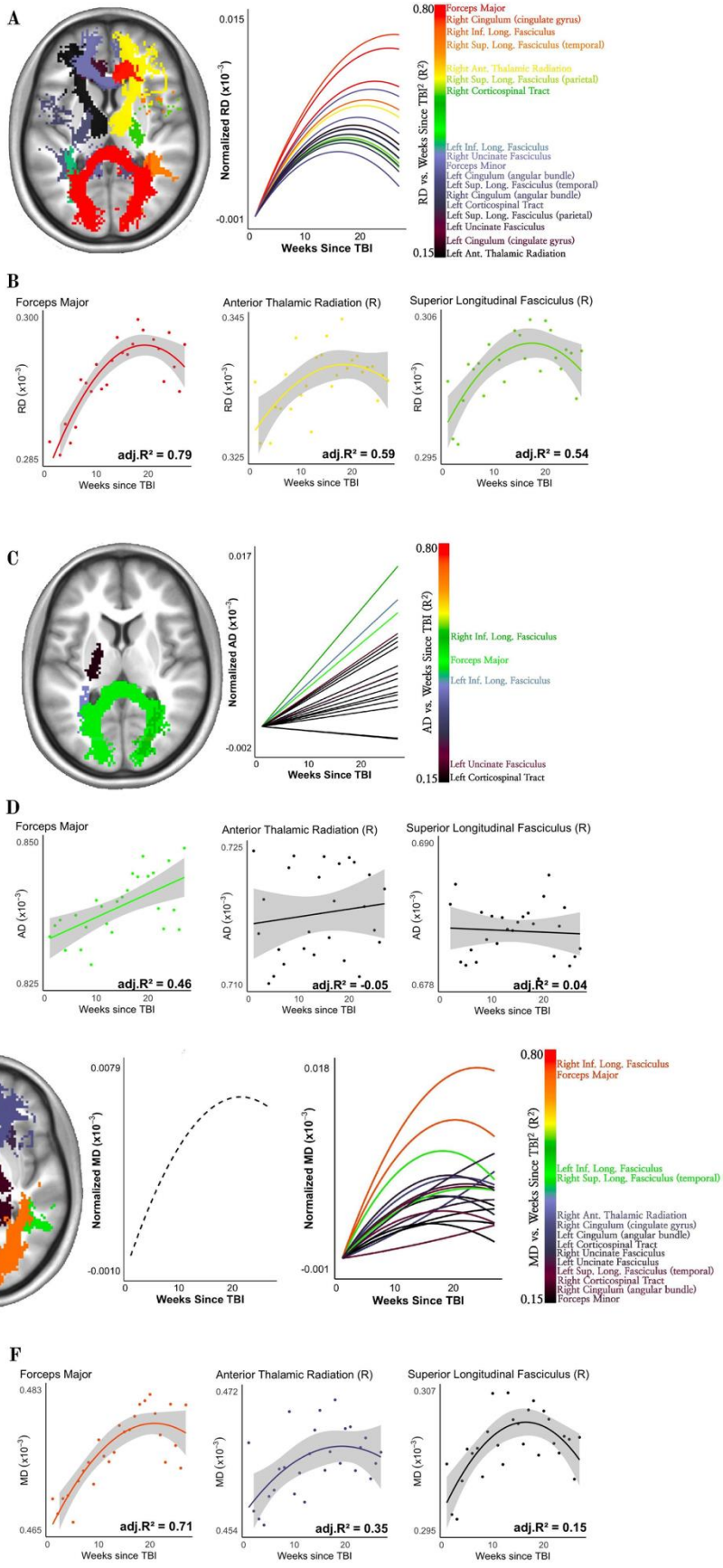
A
Normalized RD (x10⁻³)
0.015
-0.001
0
10
20
Weeks Since TBI
RD vs. Weeks Since TBI² (R²)
0.80
0.15
Forceps Major
Right Cingulum (cingulate gyrus)
Right Inf. Long. Fasciculus
Right Sup. Long. Fasciculus (temporal)
Right Ant. Thalamic Radiation
Right Sup. Long. Fasciculus (parietal)
Right Corticospinal Tract
Left Inf. Long. Fasciculus
Right Uncinate Fasciculus
Forceps Minor
Left Cingulum (angular bundle)
Left Sup. Long. Fasciculus (temporal)
Right Cingulum (angular bundle)
Left Corticospinal Tract
Left Sup. Long. Fasciculus (parietal)
Left Uncinate Fasciculus
Left Cingulum (cingulate gyrus)
Left Ant. Thalamic Radiation
B
Forceps Major
Anterior Thalamic Radiation (R)
Superior Longitudinal Fasciculus (R)
RD (x10⁻³)
0.300
0.285
0.345
0.325
0.306
0.295
adj.R² = 0.79
adj.R² = 0.59
adj.R² = 0.54
Weeks since TBI
C
Normalized AD (x10⁻³)
0.017
-0.002
Weeks Since TBI
AD vs. Weeks Since TBI (R²)
0.80
0.15
Right Inf. Long. Fasciculus
Forceps Major
Left Inf. Long. Fasciculus
Left Uncinate Fasciculus
Left Corticospinal Tract
D
Forceps Major
Anterior Thalamic Radiation (R)
Superior Longitudinal Fasciculus (R)
AD (x10⁻³)
0.850
0.825
0.725
0.710
0.690
0.678
adj.R² = 0.46
adj.R² = -0.05
adj.R² = 0.04
Weeks since TBI
E
Normalized MD (x10⁻³)
0.0079
-0.0010
0.018
-0.001
Weeks Since TBI
MD vs. Weeks Since TBI² (R²)
0.80
0.15
Right Inf. Long. Fasciculus
Forceps Major
Left Inf. Long. Fasciculus
Right Sup. Long. Fasciculus (temporal)
Right Ant. Thalamic Radiation
Right Cingulum (cingulate gyrus)
Left Cingulum (angular bundle)
Left Corticospinal Tract
Right Uncinate Fasciculus
Left Uncinate Fasciculus
Left Sup. Long. Fasciculus (temporal)
Right Corticospinal Tract
Right Cingulum (angular bundle)
Forceps Minor
F
Forceps Major
Anterior Thalamic Radiation (R)
Superior Longitudinal Fasciculus (R)
MD (x10⁻³)
0.483
0.465
0.472
0.454
0.307
0.295
adj.R² = 0.71
adj.R² = 0.35
adj.R² = 0.15
Weeks since TBI

Figure S1: Trajectories of Radial Diffusivity (RD), Axial Diffusivity (AD) and Mean Diffusivity (MD) Changes Over Weeks since TBI. (A) Left: White matter tracts in the TBI patient are colored by strength of model (quadratic) fit for RD over time (in weeks) since TBI. Tracts in orange-red indicate a strong relationship (variance explained ~80%), while tracts in purple-black indicate a weaker relationship (variance explained ~15%). Right: RD trajectories across all 18 tracts over time, based on the best-fitting quadratic model with random slope effects. RD trajectories are normalized by each tract's predicted week 1 value to enable simultaneous visualization of all tracts. RD values increase more rapidly in the early weeks post-TBI, before reversing direction, rather than following a simple linear trajectory. (B) Trajectories of RD in three example tracts: forceps major (commissural tract), right anterior thalamic radiation (projection tract), and right superior longitudinal fasciculus (association tract). (C) Left: White matter tracts for TBI patient are colored by model (linear) fit for AD over time (in weeks) since TBI. Right: AD trajectories across all 18 tracts over time, based on the best-fitting linear model with random slope effects. (D) Trajectories of AD in the same three example tracts as in (B). (E) Left: White matter tracts for TBI patient are colored by strength of model (quadratic) fit for MD over time (in weeks) since TBI. Middle: a single broken-line plot depicts the global normalized MD trajectory obtained from the mixed model, which fits a single curve by pooling across all tracts. Right: normalized MD trajectory obtained from a quadratic regression model, to illustrate the small, non-significant fluctuations across individual tracts; y-axis scaled for direct comparison with the broken-line plot. (F) Modeled MD trajectories for the same three example tracts as in (B). Across all metrics, tracts outside the 0.15-0.80 range are not represented.

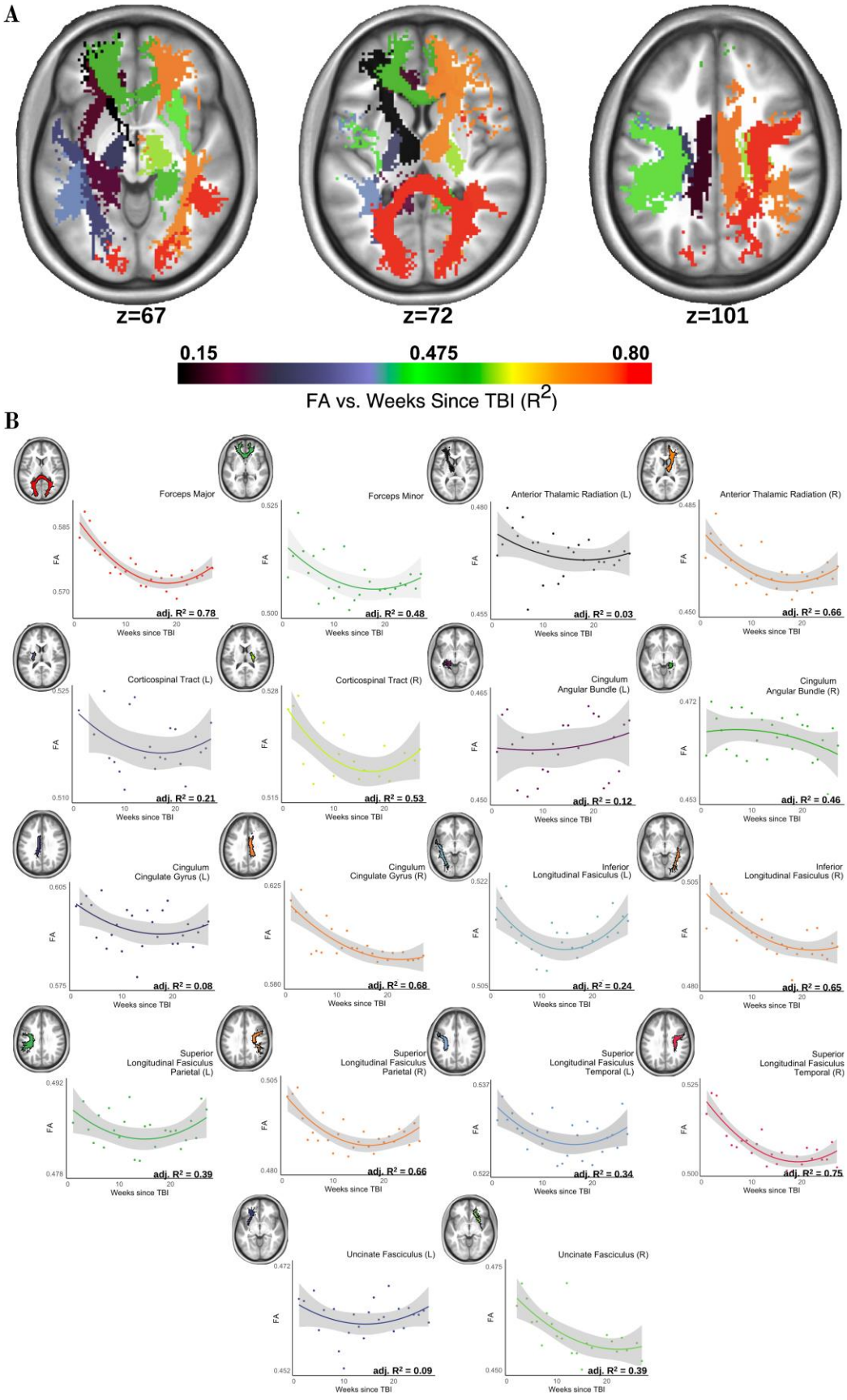
A
z=67
z=72
z=101
0.15
0.475
0.80
FA vs. Weeks Since TBI (R^2)
B
Forceps Major
adj. R^2 = 0.78
Forceps Minor
adj. R^2 = 0.48
Anterior Thalamic Radiation (L)
adj. R^2 = 0.03
Anterior Thalamic Radiation (R)
adj. R^2 = 0.66
Corticospinal Tract (L)
adj. R^2 = 0.21
Corticospinal Tract (R)
adj. R^2 = 0.53
Cingulum Angular Bundle (L)
adj. R^2 = 0.12
Cingulum Angular Bundle (R)
adj. R^2 = 0.46
Cingulum Cingulate Gyrus (L)
adj. R^2 = 0.08
Cingulum Cingulate Gyrus (R)
adj. R^2 = 0.68
Inferior Longitudinal Fasiculus (L)
adj. R^2 = 0.24
Inferior Longitudinal Fasiculus (R)
adj. R^2 = 0.65
Superior Longitudinal Fasiculus Parietal (L)
adj. R^2 = 0.39
Superior Longitudinal Fasiculus Parietal (R)
adj. R^2 = 0.66
Superior Longitudinal Fasiculus Temporal (L)
adj. R^2 = 0.34
Superior Longitudinal Fasiculus Temporal (R)
adj. R^2 = 0.75
Uncinate Fasciculus (L)
adj. R^2 = 0.09
Uncinate Fasciculus (R)
adj. R^2 = 0.39
FA
Weeks since TBI

Figure S2: Fractional Anisotropy (FA) Trajectories Across all Tracts Post-TBI. (A) Tract-wise R^2 values (quadratic model) fitting *Weeks Since TBI* against FA, visualized in three axial slices. Coordinates indicate Z slice in MNI space. (B) Trajectories of FA in all white matter tracts. In (A) and (B), each white matter tract is color-coded by R^2 value, representing the proportion of variance explained by the quadratic model.

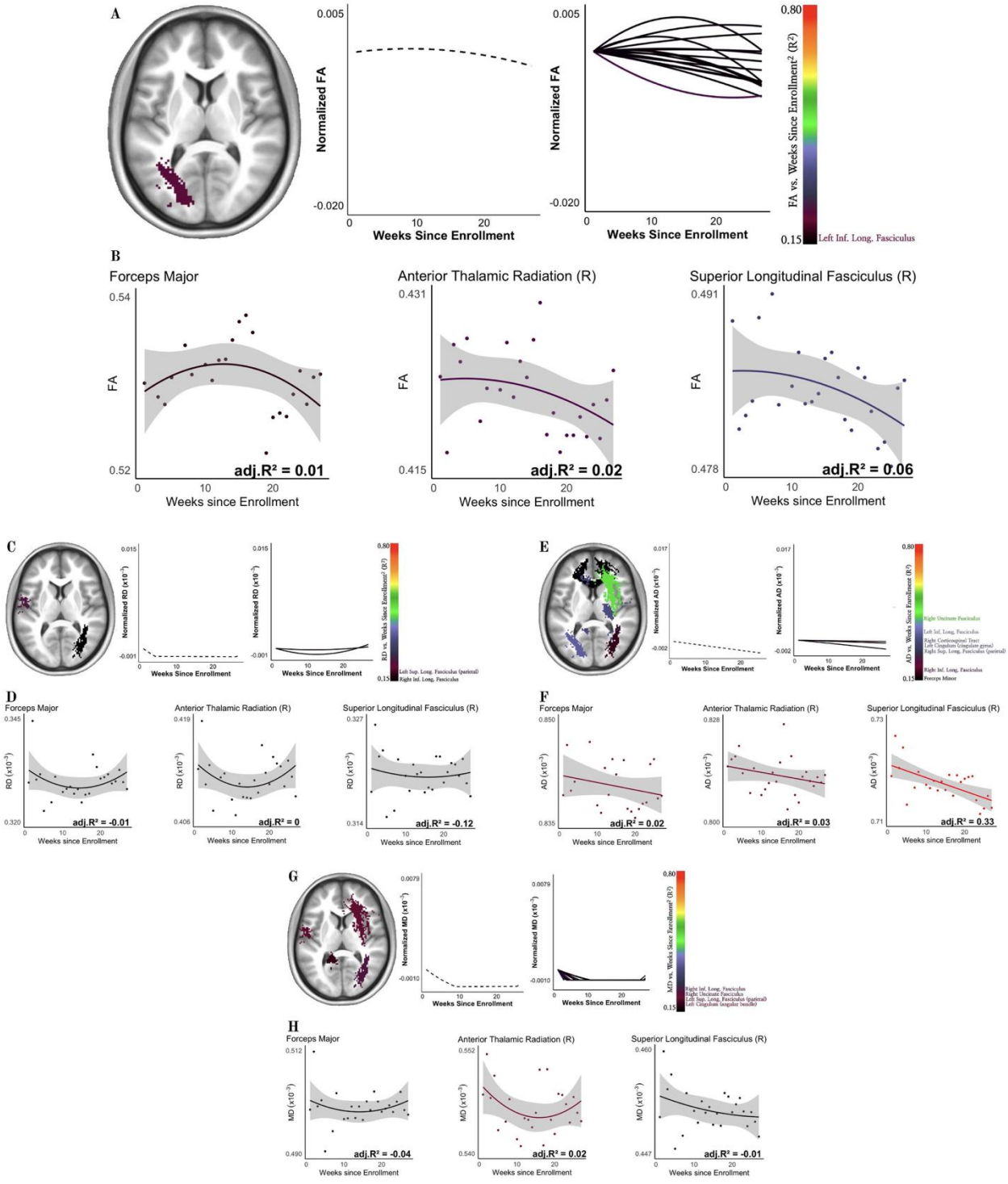

Figure S3: Trajectories of DTI Metrics over Weeks since Enrollment in the Control Participant. (A) Left: white matter tracts in the healthy control participant, colored by strength of strength of model (quadratic) fit for FA over time (in weeks) since enrollment. Middle: a single broken-line plot depicts the global normalized FA trajectory obtained from the mixed model, which fits a single curve by pooling across all tracts; y-axis scaled for direct comparison with the TBI participant. Right: normalized FA trajectory obtained from a quadratic regression model, to illustrate the small, non-significant fluctuations across individual tracts in the scaled y-axis range. (B) Modeled FA trajectories in three representative tracts chosen for direct comparison with the TBI participant (Figure 1): forceps major (commissural tract), right anterior thalamic radiation (projection tract), and right superior longitudinal fasciculus (association tract). (C) Left: white matter tracts in the healthy control are colored by strength of model (quadratic) fit for RD over time (in weeks) since enrollment, as in (A). Middle: a single broken-line plot depicts the global normalized RD trajectory obtained from the mixed model, which fits a single curve by pooling across all tracts; y-axis scaled for direct comparison with the TBI participant. Right: normalized RD trajectory obtained from a quadratic regression model, to illustrate the small, non-significant fluctuations across individual tracts in the scaled y-axis range. (D) Modeled RD trajectories for the same three example tracts as in (B). (E) Left: White matter tracts in the healthy control are colored by strength of model (linear) fit for AD over time (in weeks) since enrollment, as in A. Middle: a single broken-line plot depicts the global normalized AD trajectory obtained from the mixed model, which fits a single curve by pooling across all tracts; y-axis scaled for direct comparison with the TBI participant. Right: normalized AD trajectory obtained from a linear regression model, to illustrate the small, non-significant fluctuations across individual tracts in the scaled y-axis range. (F) Modeled AD trajectories for the same three example tracts as in (B). (G) Left: White matter tracts in the healthy control are colored by strength of model (quadratic) fit for MD over time (in weeks) since enrollment, as in A. Middle: a single broken-line plot depicts the global normalized MD trajectory obtained from the mixed model, which fits a single curve by pooling across all tracts; y-axis scaled for direct comparison with the TBI participant. Right: normalized MD trajectory obtained from a quadratic regression model, to illustrate the small, non-significant fluctuations across individual tracts in the scaled y-axis range. (H) Modeled MD trajectories for the same three example tracts as in (B). Unlike the TBI participant (Fig 1, S1), random slopes did not improve mixed model fit in the control participant, indicating minimal tract-specific variability over time. While the global mixed model curves (broken-line plots) show overall stability of DTI metrics, the tract-specific quadratic or linear fits are displayed here to illustrate the small, non-significant fluctuations across individual tracts. For clarity and comparison with the TBI participant, only tracts with fit strength within the 0.15–0.80 range are shown.

Extent of White Matter Reorganization Correlates with Duration of Change

In examining FA and RD trajectories in the TBI participant (Fig. 1A, S1B), we observed that tracts exhibiting larger deviations in FA/RD from the initial baseline also seemed to have later inflection points—that is, time points when the trajectory shifts direction (i.e., FA transitions from decline to increase and RD transitions from increase to decline). To formally test this relationship, we measured FA and RD changes up to their respective inflection points and correlated them with inflection timing. FA exhibited a significant negative correlation (Fig. 2, R=-0.67, p=0.003), indicating that tracts with later inflection points exhibited greater FA reductions. Conversely, RD exhibited a significant positive correlation (Fig. S4, R=0.71, p=0.003), indicating that tracts with later

inflection points exhibited greater RD increases. These results suggest that when the post-TBI white matter remodeling process is more extensive, that process is also more temporally extended.

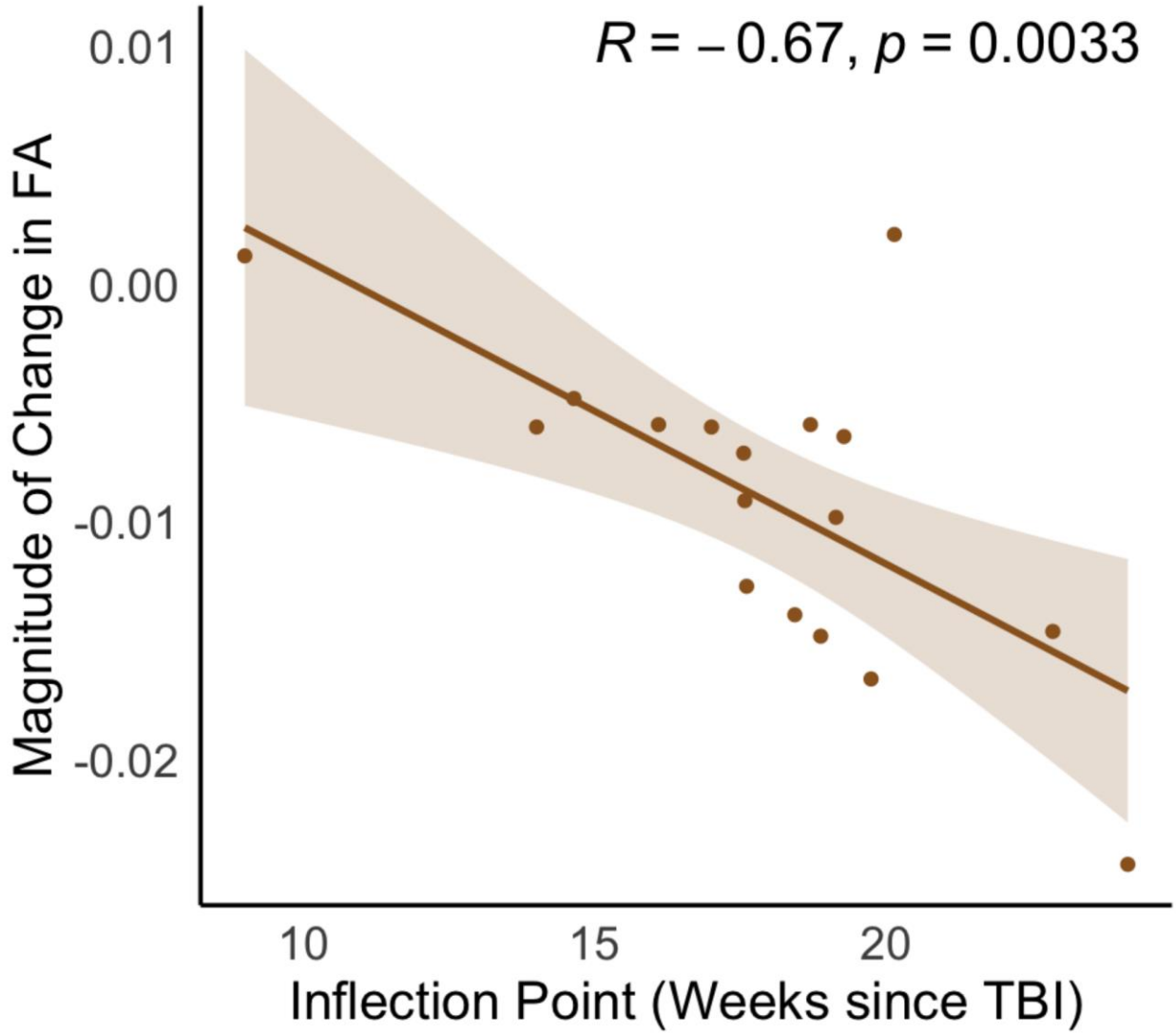

Figure 2. Relationship Between Inflection Point Timing and Magnitude of Change in FA. Scatter plot showing the negative correlation between the inflection point timing and the magnitude of change in fractional anisotropy (FA; R = -0.67, p = 0.0033). Later inflection points are associated with greater FA reductions before stabilization. Shaded areas represent 95% confidence intervals.

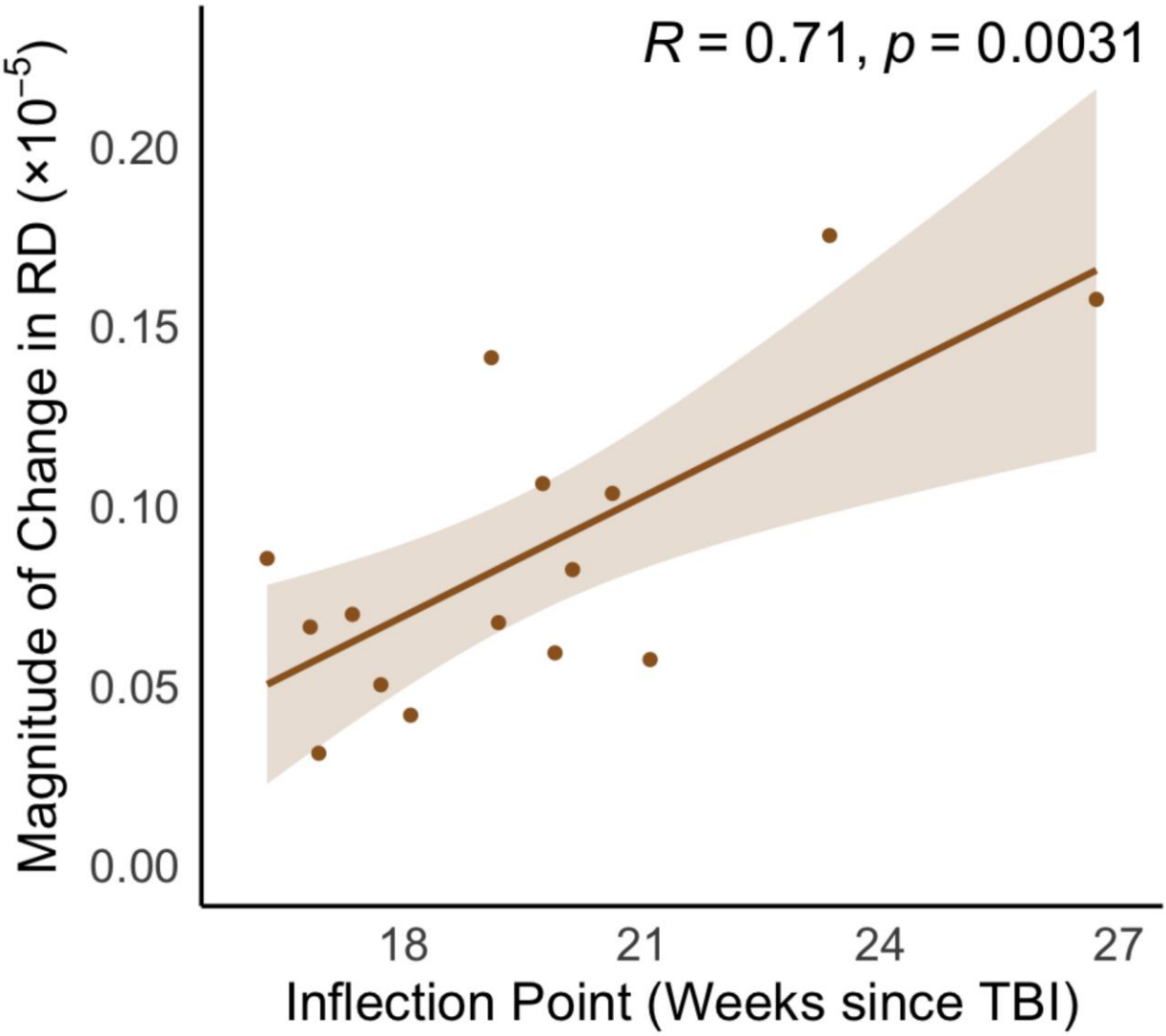

Figure S4. Relationship Between Inflection Point Timing and Magnitude of Change in RD. Scatter plot showing the positive correlation between the inflection point timing and the magnitude of change in radial diffusivity (RD; R = 0.71, p = 0.0031). Later inflection points are linked to greater RD increases before stabilization. Shaded areas represent 95% confidence intervals.

White Matter Trajectories correspond with Recovery of Cognitive and Emotional Processes After TBI

Cognitive and emotional functions are often immediately impacted by TBI but can eventually recover. To assess whether changes in white matter contribute to cognitive and emotional recovery following TBI, we examined whether trajectories of DTI measures mediate improvements in Number-Symbol task performance and reductions in anxiety and depression symptoms over time.

In the TBI patient, we observed that reaction times in the Number-Symbol task improved over time (Fig 3A), with a curvilinear trajectory that generally followed the

trajectory of DTI changes (Fig 1). However, reaction times on cognitive tasks often improve with repeated administration due to practice effects (Bartels et al., 2010; Holm et al., 2022; Cook, Ramsay, & Fayers, 2004). Indeed, a similar trajectory of improvement was observed in the control participant (Fig 3B).

To test whether these reaction time improvements depended on white matter changes, we used a quadratic mediation network. To ensure statistical robustness, mediation models were bootstrapped 5000 times. For the TBI patient, FA in the left inferior longitudinal fasciculus (ILF) showed a significant indirect effect ($\beta_{Indirect} = 0.13,\ \mathrm{p} = 0.03$), while the direct effect remained negative and significant ($\beta_{Direct} = -0.88,\ \mathrm{p} < 0.001$), yielding a total effect of $\beta_{Total} = -0.75\ (\ \mathrm{p} < 0.001$). The proportion mediated was -17.3% (p = .03), suggesting that reductions in FA in the left ILF during recovery contributed to greater cognitive improvement than would be expected based on time alone (Fig 3C). In the right ILF, both RD and MD showed a significant indirect effect ($\beta_{Indirect} = -0.18,\ \mathrm{p} = 0.01\ \text{for both metrics}$), alongside a significant direct effect ($\beta_{Direct} = -0.56\ \text{and}\ \beta_{Direct} = -0.58\ \text{respectively},\ \mathrm{p} < 0.001$) with total effects of $\beta_{Total} = -0.75\ \text{and}\ \beta_{Total} = -0.76\ \text{respectively}\ (\mathrm{p} < 0.001)$. The proportion mediated was 24.6% (p = .01) for RD and 23.8% (p=0.01) or MD, indicating partial associative mediation. These findings suggest that structural changes in white matter reflect the trajectory of cognitive recovery.

In contrast, although the direct effect of time on RT in the control participant was highly significant (β = -0.78 to -0.96, p < 0.001), no significant mediation effect was observed (Fig 3D), as reaction time improvements occurred independently of any change in any DTI metric (FA, RD, AD, or MD). Across all tracts, indirect effects ranged from -0.06 to 0.09 and proportion mediated estimates ranged from 0% to 7.5%, with all p-values non-significant (p = 0.13–0.98), indicating no evidence of mediation.

To ensure that the mediation effects were not dependent on the specific choice of nonlinear modeling, we conducted a parallel mediation analysis using linear models, modeling all DTI metrics and reaction time as linear functions of weeks since TBI (or weeks since enrollment). This analysis replicated the quadratic mediation findings and identified additional tract-level contributions, including the forceps major as well as the right inferior and superior longitudinal fasciculus, suggesting more widespread white matter involvement in cognitive recovery (Table 2).

We further examined recovery of emotional processes following TBI. Anxiety symptoms showed a sustained reduction, following a similar trajectory to DTI measures, while depression symptoms rebounded earlier (Fig S5). Only a linear mediation model yielded significant effects of white matter involvement in post-TBI recovery of emotional symptoms. Specifically, RD and MD in the forceps major ($\beta_{Indirect}$ = -0.48, *p* = .02; $\beta_{Indirect}$ = -0.46, *p* = .01, respectively), mediated 85.4% and 82.4% of the total effect (*p* = .03 and *p* = .02). FA and RD in the superior longitudinal fasciculus ($\beta_{Indirect}$ = -0.42, *p* = .04; $\beta_{Indirect}$= -0.46, *p* = .01, respectively), mediated 72.4% and 80.8% of the total

effect (p = .04 and p = .02). FA, RD, and MD in these tracts *fully mediated* reductions in anxiety. Notably, the same tracts implicated in cognitive improvements—the forceps major and superior longitudinal fasciculus—also mediated reductions in anxiety symptoms (Table 2), suggesting overlapping white matter mechanisms underlying both cognitive and anxiety recovery. No significant mediation effects were found for depression symptoms. See Table 2 for full mediation statistics.

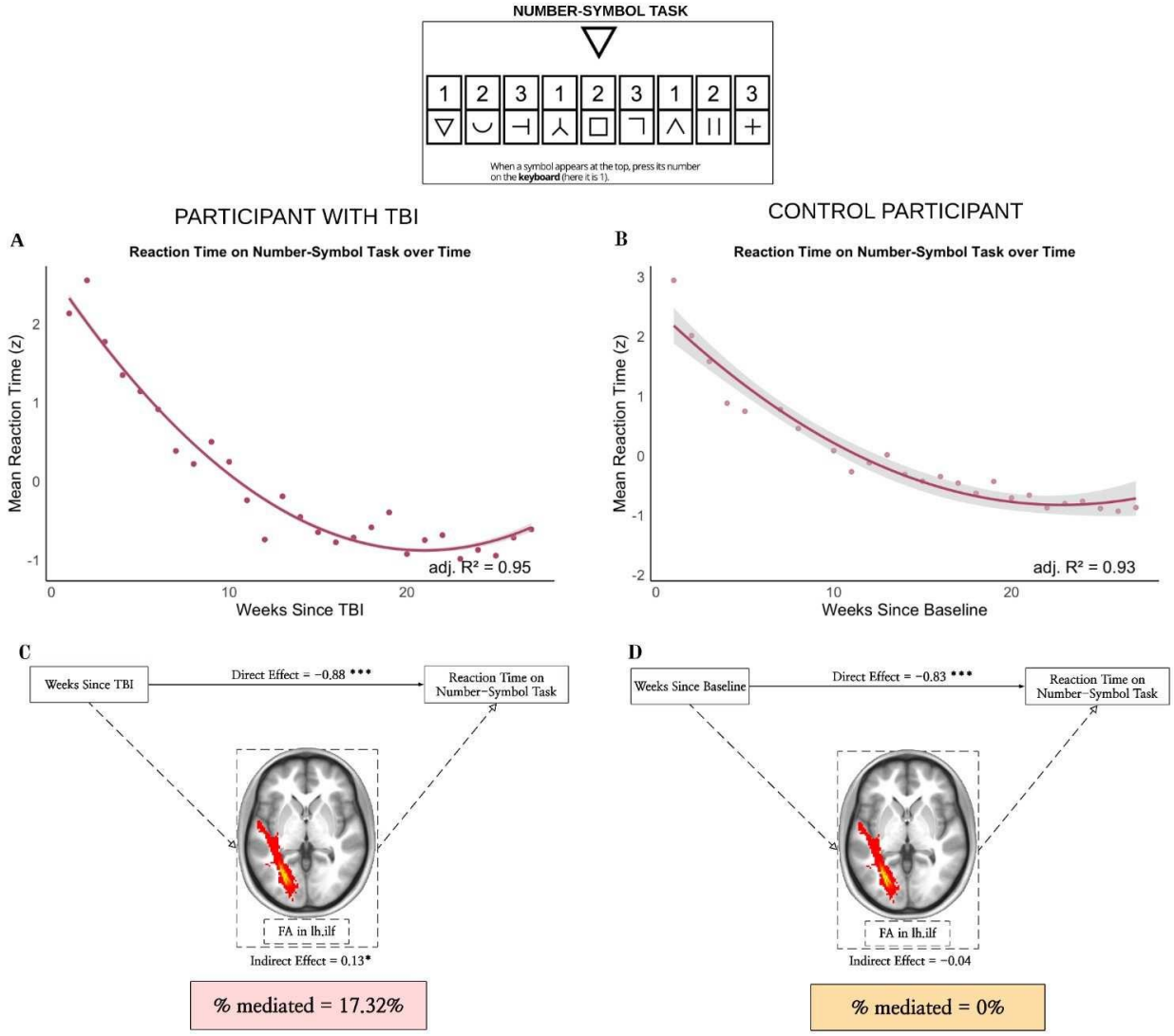

Figure 3: Cognitive Improvements on the Number-Symbol Task Mediated by White Matter-Driven Recovery in TBI. Both the participant with TBI (A) and control participant (B) improved on the number-symbol cognitive task over time, with reaction times decreasing rapidly in the early weeks before stabilizing. To determine whether these improvements reflect practice effects (due to repeated exposure) or longitudinal recovery effects (linked to TBI-related white matter changes), we tested this relationship within a causal mediation framework. In the participant with TBI (C), time since injury strongly predicted faster reaction times (negative direct effect). However, mediation analysis revealed that lower fractional anisotropy (FA) in the left inferior longitudinal fasciculus (ILF) partially enhanced (17%) the beneficial direct effect of weeks since TBI on cognitive improvement. Thus, reductions in FA during recovery contributed to greater cognitive improvement than would be expected by time alone. This mediation effect

was completely absent in the control participant (D; mediation effect = 0%), where reaction time improvements occurred independently of white matter changes.

Table 2: Linear Mediation Models for Reaction Time Performance on Number-Symbol task and Mean Anxiety levels on Beck Anxiety Inventory

TRACT	Outcome	Metric	Direct Effect	Indirect Effect	Proportion Mediated (%)	Mediation Strength
Forceps Major	Cognitive Performance	FA	-0.6***	-0.3***	37.5	Partial
		RD	-0.5***	-0.4***	41.9	Partial
		MD	-0.6***	-0.3***	28.8	Partial
	Anxiety Level	RD	-0.1	-0.5*	85.4	**Full**
		MD	-0.1	-0.5*	82.4	**Full**
Sup. Long. Fasciculus-Temporal (R)	Cognitive Performance	FA	-0.6***	-0.3*	36.0	Partial
		RD	-0.6***	-0.3*	34.0	Partial
	Anxiety	FA	-0.2	-0.4*	36.0	**Full**
		RD	-0.1	-0.5*	80.8	**Full**
Inf. Long. Fasciculus (R)	Cognitive Performance	FA	-0.6***	-0.3***	28.8	Partial
		RD	-0.6***	-0.3***	36.0	Partial
		MD	-0.6***	-0.3***	33.9	Partial
	Anxiety	MD	-0.1	-0.5*	84.7	**Full**
Sup. Long. Fasciculus-Parietal (R)	Cognitive Performance	FA	-0.7***	-0.2*	18.4	Partial
		RD	-0.8***	-0.1*	14.3	Partial
Inf. Long. Fasciculus (L)	Cognitive Performance	RD	-0.5***	-0.4***	41.9	Partial
Uncinate Fasciculus (L)	Cognitive Performance	MD	-0.8***	-0.1***	13.6	Partial

Table 2: Statistically significant results from linear mediation models assessing how DTI metrics mediate cognitive and emotional outcomes post-TBI. The models examine the relationship between weeks since TBI and (1) reaction time performance on the Number-Symbol task (cognitive outcome) and (2) mean anxiety levels (emotional outcome), with mediation effects assessed through fractional anisotropy (FA), radial diffusivity (RD), axial diffusivity (AD), mean diffusivity (MD). No mediation effects for AD were found for any tract or outcome. Mediation effects were categorized as either partial (when indirect effects explained part of the relationship between weeks since TBI and outcome) or full (when indirect effects through the DTI metrics accounted for most of the observed association). Statistical significance is denoted as $p<0.05$ (*) and $p < 0.001$(***). FA and RD predominantly mediated cognitive outcomes, with partial mediation observed in the forceps major, right superior longitudinal fasciculus (temporal and

parietal projections), bilateral inferior longitudinal fasciculus, and left uncinate fasciculus. RD and MD primarily mediated anxiety levels, with full mediation observed in the forceps major, right superior longitudinal fasciculus (temporal projections), and right inferior longitudinal fasciculus.

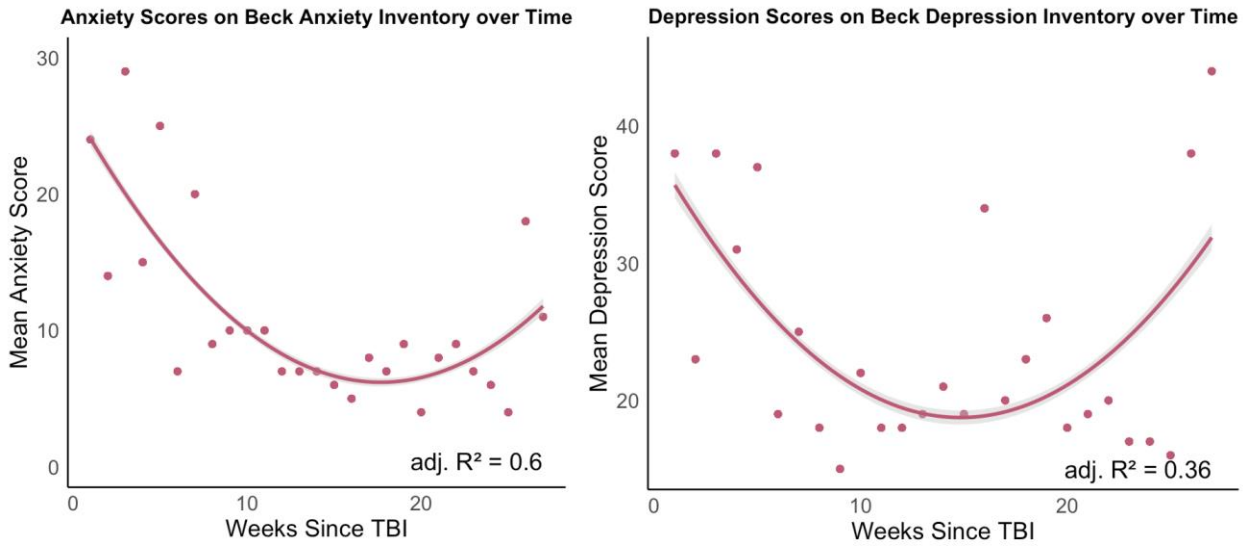

Figure S5. Trajectories of Anxiety and Depression Symptoms Following TBI. Mean anxiety (left) and depression (right) scores over 27 weeks post-TBI, assessed using the Beck Anxiety Inventory (Beck, Epstein, Brown, & Steer, R., 1993) and Beck Depression Inventory (Beck, Steer, & Brown, 1996) respectively. Both symptoms followed a quadratic trajectory, with anxiety scores declining sharply before stabilizing, whereas depression scores exhibited a U-shaped pattern, initially improving before later rebounding. Adjusted R^2 values indicate a stronger fit for anxiety ($R^2 = 0.6$) than depression ($R^2 = 0.36$), suggesting that anxiety reductions may follow a more predictable course, while depression symptoms may be more variable over time.

Characterization of White Matter Recovery Using DBSI: Linking Structural, Inflammatory, and Vascular Mechanisms Post-TBI

To disaggregate the complex microstructural changes following TBI, we leveraged DBSI to capture distinct biological processes such as axonal integrity, neuroinflammation, and vascular contributions that are not fully disambiguated by DTI (Wang et al., 2019a, 2015, 2011). DBSI metrics can more specifically distinguish the separate biophysical effects on water diffusion caused by fiber loss or demyelination, inflammation, edema, and vascular changes (Wang et al., 2015, 2014, 2011, Chiang et al., 2014). DBSI metrics—including fiber ratio, cellularity ratio, free water ratio, hindered ratio, and perfusion ratio—were extracted from 18 major white matter tracts. Longitudinal trajectories were modeled over the 27 weeks post-TBI to assess distinct recovery patterns.

We again used mixed-effects models that incorporated either a linear or quadratic term for weeks since TBI, assessing how Weeks since TBI influenced changes in each DBSI metric. Quadratic models provided a significantly better fit than

linear models for fiber ratio, cellularity ratio, and free water ratio (ps < 10^{-8}, ΔAIC > 10; Table 1). In contrast, for hindered ratio and perfusion ratio, although the quadratic models were not significantly worse (p = 0.25 and p = 0.22), the ΔAIC differences were minimal (ΔAIC = 1), and following principles of model parsimony, the simpler linear model was preferred.

The nonlinear models explained a moderate amount of variance across tracts, averaging ~10% for fiber ratio, 24% for cellularity ratio, and 16% for free water ratio. Notably, the right cingulum showed strong quadratic effects for both fiber (R^2 = 0.51) and free water (R^2 = 0.60) ratios, while the forceps major exhibited the strongest effect for cellularity (R^2 = 0.66). In contrast, linear models explained only 10% of the variance across tracts for hindered ratio and 7% for perfusion ratio.

Fiber ratio—which indexes axonal integrity and alignment—showed an inverted U-shaped trajectory with early increases followed by later decline. Cellularity ratio—a marker of inflammatory and glial cell presence—exhibited a U-shaped course with early decreases and later rebound. Free water ratio—which reflects extracellular space available for water diffusion—also followed a U-shaped trajectory with early reductions and subsequent recovery. Hindered ratio—an index of edema-related extracellular water—increased linearly across time. Perfusion ratio—reflecting microvascular contributions—declined linearly and remained persistently low (Fig 4, Table 1).

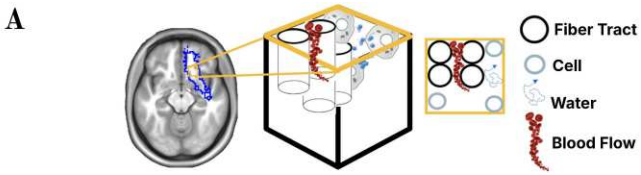
A
Fiber Tract
Cell
Water
Blood Flow

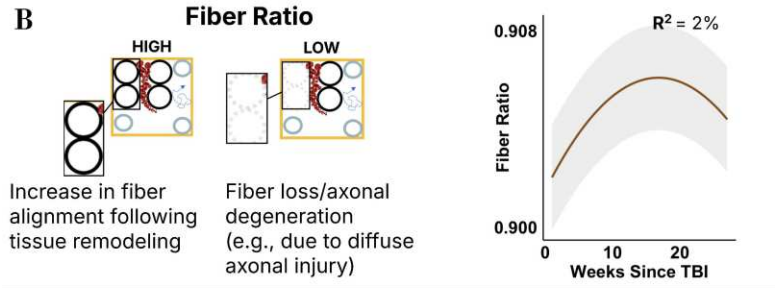
B
Fiber Ratio
HIGH
LOW
Increase in fiber alignment following tissue remodeling
Fiber loss/axonal degeneration (e.g., due to diffuse axonal injury)
R² = 2%
0.908
Fiber Ratio
0.900
0
10
20
Weeks Since TBI

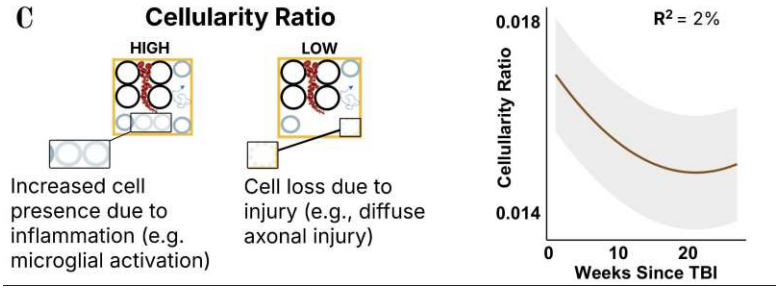
C
Cellularity Ratio
HIGH
LOW
Increased cell presence due to inflammation (e.g. microglial activation)
Cell loss due to injury (e.g., diffuse axonal injury)
R² = 2%
0.018
Cellularity Ratio
0.014
0
10
20
Weeks Since TBI

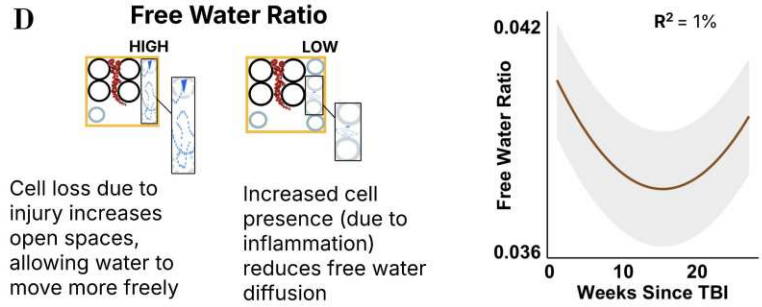
D
Free Water Ratio
HIGH
LOW
Cell loss due to injury increases open spaces, allowing water to move more freely
Increased cell presence (due to inflammation) reduces free water diffusion
R² = 1%
0.042
Free Water Ratio
0.036
0
10
20
Weeks Since TBI

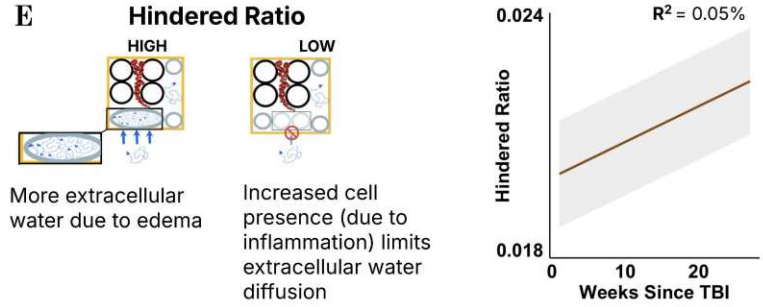
E
Hindered Ratio
HIGH
LOW
More extracellular water due to edema
Increased cell presence (due to inflammation) limits extracellular water diffusion
R² = 0.05%
0.024
Hindered Ratio
0.018
0
10
20
Weeks Since TBI

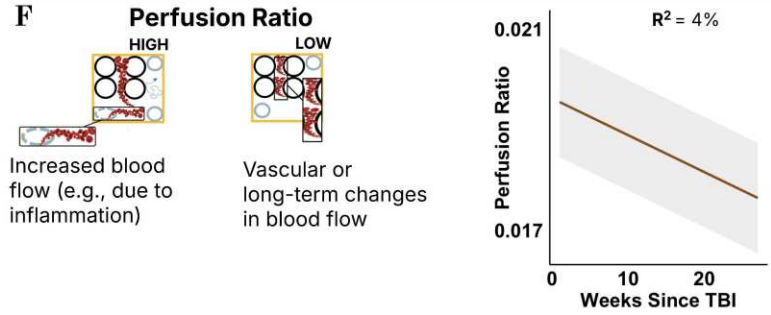
F
Perfusion Ratio
HIGH
LOW
Increased blood flow (e.g., due to inflammation)
Vascular or long-term changes in blood flow
R² = 4%
0.021
Perfusion Ratio
0.017
0
10
20
Weeks Since TBI

Figure 4. DBSI Metrics Exhibit Post-TBI Recovery Trajectories. A: representation of a white matter tract (outlined in blue) and a single voxel (cube), illustrating how diffusion signals are influenced by multiple biophysical factors at the cellular level, which can be differentiated using Diffusion Basis Spectrum Imaging (DBSI). B. *Fiber Ratio*: Left—A high Fiber Ratio indicates well-aligned fibers, while a reduction suggests axonal degeneration or demyelination, as observed in diffuse axonal injury. Right—Following TBI, Fiber Ratio initially increases before declining, potentially reflecting a transient prominence of axonal fibers in the diffusion signal before later structural remodeling. C. *Cellularity Ratio*: Left—An increase in cellularity corresponds to immune cell infiltration, indicative of an inflammatory response, while a decrease suggests cell loss. Right—Cellularity initially declines post-TBI, likely due to early cell loss, before rebounding over time, suggesting neuroinflammatory responses and tissue remodeling. D. *Free Water Ratio*: Left—Intracellular free water levels increase with cell loss and decrease with inflammation-driven cell accumulation. Right—The Free Water Ratio follows a U-shaped trajectory over time, initially decreasing before increasing again, likely due to evolving edema and tissue remodeling. E. *Hindered Water Ratio*: Left—Extracellular water movement increases with edema-related swelling, while inflammation driven cell accumulation decreases extracellular water movement. Right—The Hindered Water Ratio shows a small increase over time, suggesting progressive microstructural alterations that facilitate more intracellular water movement. F. *Perfusion Ratio*: Left—Elevated perfusion suggests increased blood flow due to inflammation, whereas a reduction may indicate vascular remodeling or long-term changes in cerebral blood flow. Right—The Perfusion Ratio declines progressively post-TBI, indicating potential reductions in inflammation-driven hyperemia or long-term microvascular alterations. Each graph presents longitudinal trajectories of these DBSI-derived metrics across weeks post-TBI, with shaded regions representing confidence intervals. In each graph, R^2 values indicate marginal effects, i.e., the proportion of variance explained only by the fixed effects (i.e., weeks since TBI, head motion, and for quadratic models, weeks since TBI^2).

Non-linear Recovery of FA and RD at 1-year follow-up

To assess whether white matter recovery was complete at the tract level, we extended the quadratic trajectories modeled during the first six months post-injury to estimate when each tract's diffusion metrics (FA and RD) were expected to return to early post-injury baseline values. We then compared these predicted recovery trajectories to the diffusion values observed at the one-year follow-up, allowing us to evaluate whether each tract successfully recovered by one-year post-injury relative to its initial expected trajectory (Fig. 5A, S6A; for tract-wise trajectories, see Fig. S7).

Most tracts fell within the 95% confidence interval (CI) of the predicted baseline at one year, consistent with full recovery (Fig 5A, green; Fig S6, green). In contrast, others—particularly the right cingulum bundle (r.cing, Fig 5A, S6), right inferior and superior longitudinal fasciculus (r.ilf, Fig S6; r.slft, Fig 5A, S6), and right anterior thalamic radiation (Fig S6) —exhibited persistent deviations from baseline at one-year follow-up, suggesting incomplete recovery. Notably, most non-recovered tracts were right-lateralized, consistent with the patient's right temporal subdural hematoma.

We next asked whether the magnitude of early structural alteration predicted the degree of recovery. To test this, we correlated the initial change in FA and RD (baseline to vertex) with the deviation from baseline at one year (Fig 5B, S6B). We found that tracts with larger changes before the inflection point exhibited significantly larger

deviations from baseline at one year, for both FA ($R = 0.55$, $p = 0.02$; Fig 5B) and RD ($R = 0.82$, $p = 0.0002$; Fig S6B). These findings suggest that the extent of early white matter disruption may constrain the completeness of recovery over time.

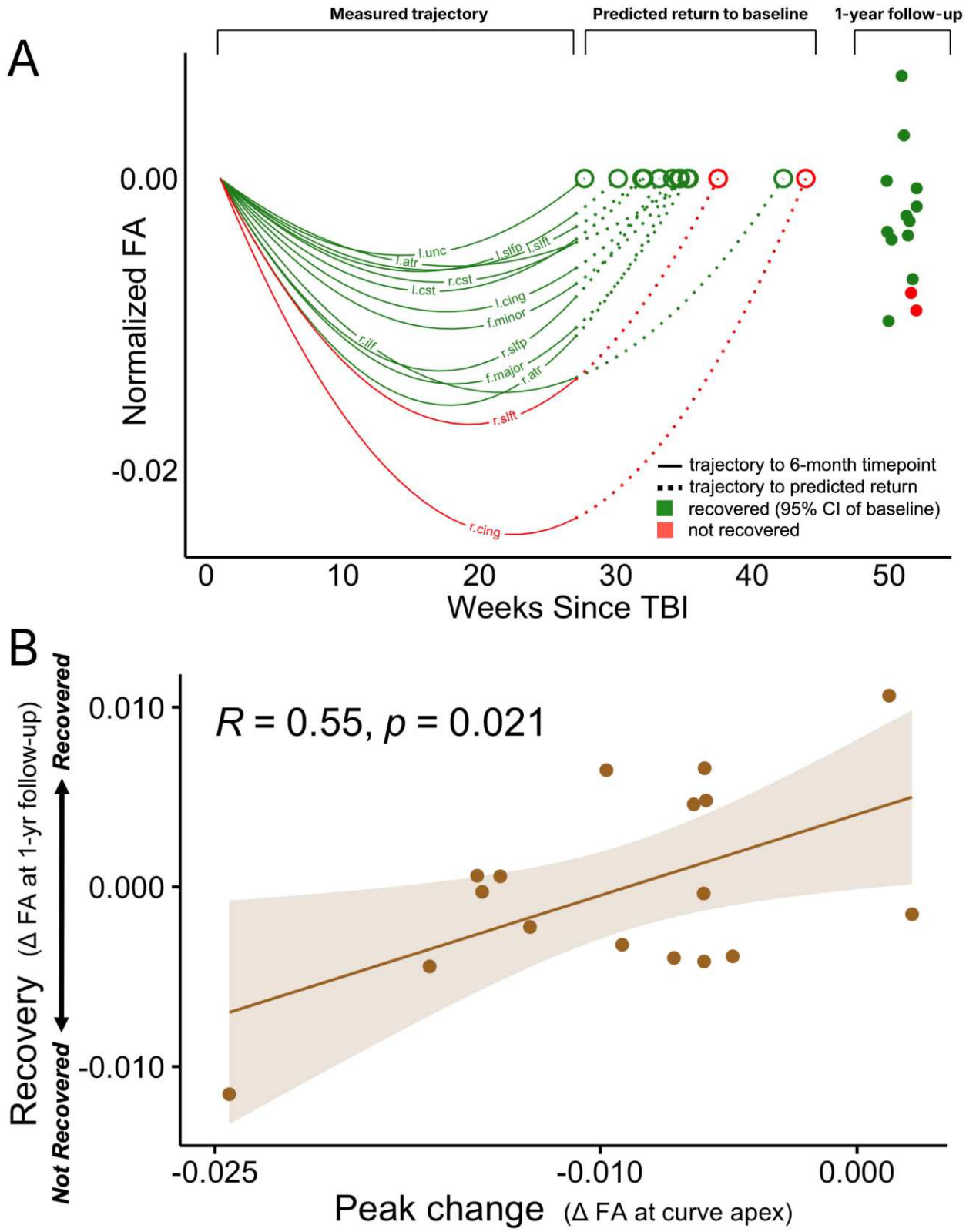

Figure 5. Tract-specific white matter recovery trajectories and their relation to early disruption in fractional anisotropy (FA). (A) Normalized FA values were modeled

using quadratic functions fit to densely sampled data from the first six months post-injury. Each curve reflects a predicted recovery trajectory for a tract, anchored to early post-injury baseline values (Week 1). Hollow circles mark the predicted timepoints when FA was expected to return to baseline, and solid dots show the observed FA at one year (Week 51). Tracts where 1-year values fell within the 95% confidence interval (CI) of the predicted return are shown in green (“Recovered”); those falling outside the CI are shown in red (“Not Recovered”). Notably, the right corticospinal tract (r.cst) showed a 1-year value above rather than below the predicted CI but was still classified as “Recovered” given that it exceeded the expected return. Dotted lines indicate the extrapolated trajectory from the last observed timepoint to the predicted return. Only tracts with predicted return-to-baseline times between 6 months and 1-year post-injury are included for interpretability. (B) Greater early disruption in FA was associated with more persistent alteration at 1 year. The x-axis represents the magnitude of early change in FA, calculated as the difference between baseline (Week 1) and the vertex (i.e., the minimum FA within the first 6 months). The y-axis shows deviation from baseline at 1 year. A significant positive correlation ($R = 0.55$, $p = 0.021$) suggests that tracts with larger early FA declines tend to show less complete recovery by one year. Shaded region denotes the 95% confidence interval.

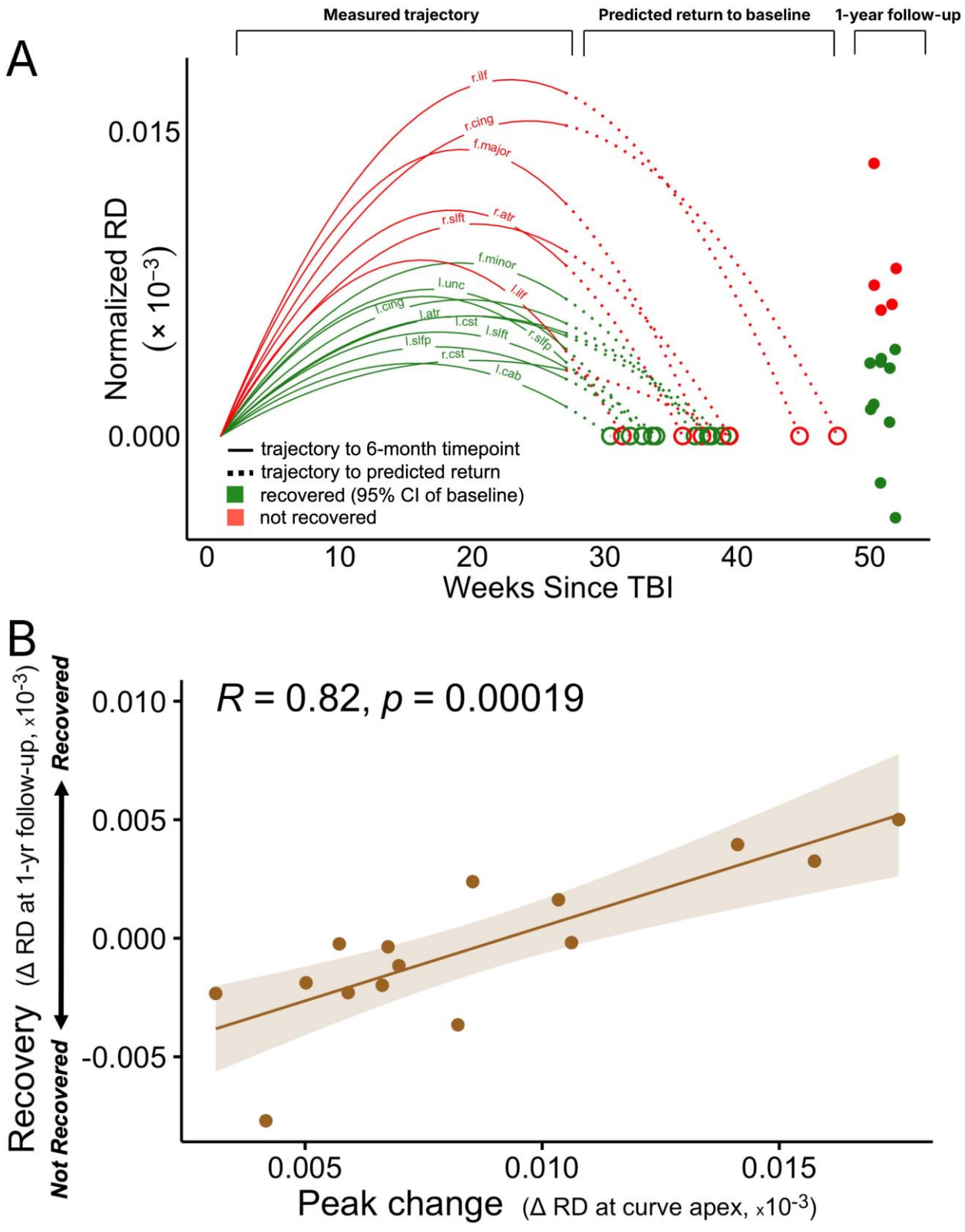
A
Measured trajectory
Predicted return to baseline
1-year follow-up
Normalized RD
(× 10⁻³)
0.015
0.000
r.ilf
r.cing
f.major
r.slft
r.atr
f.minor
l.unc
l.ilf
l.cing
l.atr
l.cst
l.slft
r.slfp
l.slfp
r.cst
l.cab
trajectory to 6-month timepoint
trajectory to predicted return
recovered (95% CI of baseline)
not recovered
0
10
20
30
40
50
Weeks Since TBI
B
R = 0.82, p = 0.00019
Recovery (Δ RD at 1-yr follow-up, x10-3)
Recovered
Not Recovered
0.010
0.005
0.000
-0.005
0.005
0.010
0.015
Peak change (Δ RD at curve apex, x10-3)

Figure S6. Tract-specific white matter recovery trajectories and their relation to early disruption in radial diffusivity (RD). (A) Normalized RD values were modeled using quadratic functions fit to densely sampled data from the first six months post-injury. Each curve reflects a predicted recovery trajectory for a tract, anchored to early post-injury baseline values (Week 1). Hollow circles mark the predicted timepoints when RD was expected to return to baseline, and solid dots show the observed RD at one year (Week 51). Tracts where 1-year values fell within the 95% confidence interval (CI) of the predicted return are shown in green ("Recovered"); those falling outside the CI are shown in red ("Not Recovered"). Dotted lines indicate the extrapolated trajectory from the last observed timepoint to the predicted return. Only tracts with predicted return-to-baseline times between 6 months and 1-year post-injury are included for interpretability. (B) Greater early disruption in RD was associated with more persistent alteration at 1 year. The x-axis represents the magnitude of early change in RD, calculated as the difference between baseline (Week 1) and the vertex (i.e., the maximum RD within the first 6 months). The y-axis shows deviation from baseline at 1 year. A significant positive correlation ($R = 0.82$, $p = 0.00019$) suggests that tracts with larger early increases in RD tend to show less complete recovery by one year. Shaded region denotes the 95% confidence interval.

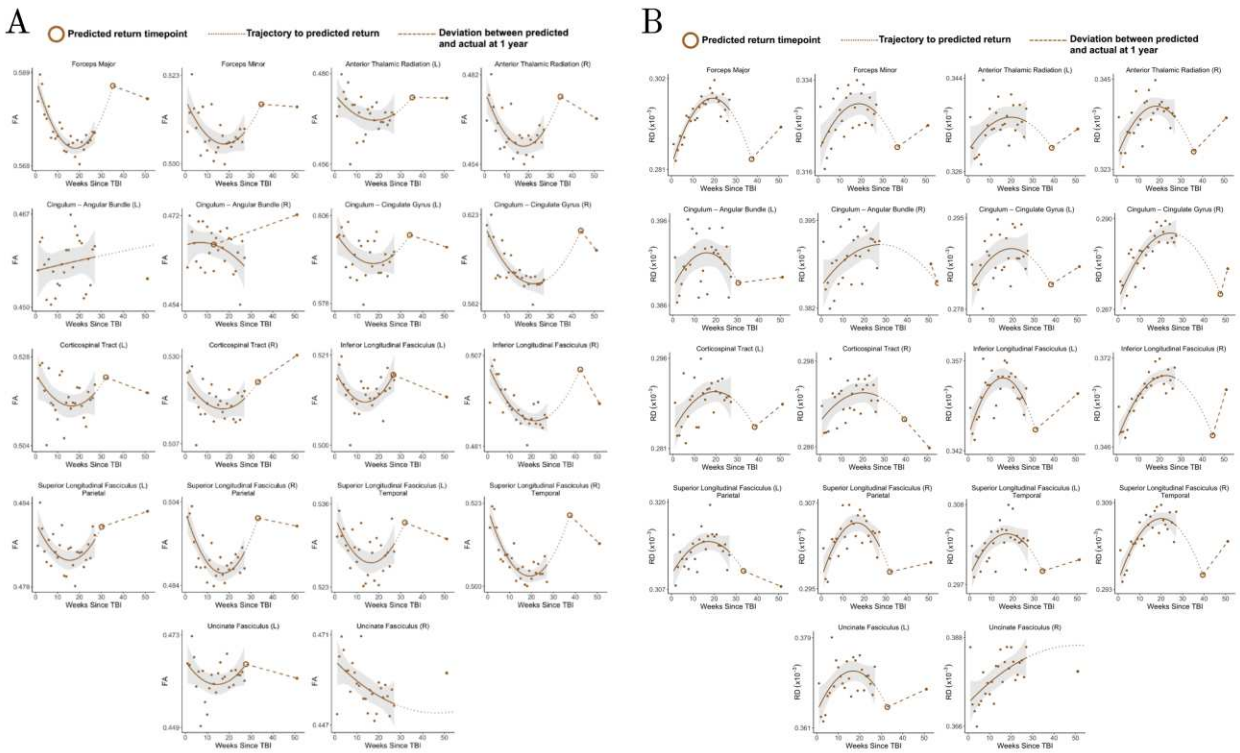

Figure S7: (A)Fractional anisotropy (FA) and (B)radial diffusivity (RD) trajectories across all modeled white matter tracts. Each subplot depicts the modeled trajectory for one tract, normalized to the Week 1 post-injury baseline. The dotted line represents the extrapolated trajectory from the last observed 6-month timepoint to the predicted return to baseline, indicated by a hollow circle. The dashed line reflects the deviation between the predicted return and the observed value at one year (Week 51), marked by a solid dot.

Discussion

This densely sampled, precision longitudinal study aimed to elucidate the individual-level trajectory of white matter remodeling following traumatic brain injury. We found that DTI measures—particularly FA and RD—follow a non-linear, parabolic trajectory over the first year (Fig 1, S1). Complementary DBSI-analyses suggested early cell loss followed by inflammatory processes, leading to persistent microvascular alterations in white matter (Fig 4). These neurobiological changes were not static snapshots of damage; they tracked closely with cognitive recovery and anxiety symptoms (Fig 3, Table 2), reinforcing the functional significance of microstructural remodeling.

Despite growing recognition of white matter plasticity post-TBI, recovery is still often interpreted through rigid and inconsistently defined subacute (> 1 week to ≤ 3months) and chronic (>3 months) phases (Wallace, Mathias, & Ward, 2018). The absence of clear differentiation in the underlying neurobiological processes and recovery dynamics across these intervals raises the question of whether these categories are biologically meaningful or merely artifacts of inconsistent definitions. Rather than adhering to fixed post-injury windows, our findings suggest that white matter recovery is neither staged nor linear, but unfolds along dynamic, tract-specific trajectories (Fig 1, S1, S2). Across tracts, we identified discrete inflection points—defined as the time at which diffusion metrics (FA and RD) reversed direction—marking a pivot from early structural alteration toward potential reorganization and recovery. These inflection points varied widely: for FA, they ranged from ~13 weeks (e.g., left cingulum angular bundle, projecting to the angular gyrus) to ~27 weeks (e.g., right cingulum bundle within the cingulate gyrus); for RD, from ~16 to ~26 weeks within the same white matter tracts. This variability underscores that recovery begins on different biological timelines across the brain.

Importantly, the timing of these shifts was not arbitrary. Tracts with greater early deviation from baseline tended to show later inflection points (Fig 2) and more persistent abnormalities at one year (Fig 5, S6), suggesting that the degree of initial structural alteration may delay the onset and limit the extent of recovery. Notably, several tracts showing incomplete recovery were right-lateralized (e.g., right inferior longitudinal fasciculus; Fig 5A, B; Fig S6A, B)—that is, located on the same side as the patient's right temporal subdural hematoma. This pattern raises the possibility that recovery trajectories may also reflect hemisphere-specific vulnerability. More broadly, these findings support the view that recovery phases are shaped not by time alone, but by the degree of remodeling each tract must undergo.

Together, these observations offer a biologically grounded, individualized framework for tracking white matter repair. While symptom resolution is often used as a proxy for recovery, it provides no direct insight into the underlying state of neural tissue. Our findings show that structural abnormalities may persist even when overt clinical

symptoms subside, reinforcing long-standing concerns about post-injury vulnerability periods, such as those implicated in repeated head trauma (Mouzon et al., 2018; Buki et al., 2014), which often go undetected by behavioral metrics alone (Buki et al., 2014). In contrast, modeling white matter recovery at the tract level provides a more granular index of neural resilience and can reveal lingering microstructural vulnerabilities that might otherwise be missed.

By linking the timing of recovery to the extent of early structural alterations and how far these changes remain from their post-injury baseline, we move toward a more precise, biologically grounded model of post-TBI repair. This tract-informed approach avoids reliance on static phase labels such as “subacute” and “chronic”, and instead allows for individualized monitoring of white matter recovery. Clinically, such tract-level markers could inform decisions about when it is biologically safe to resume daily activities—a critical challenge in post-TBI care that currently lacks objective guidance (Silverberg & Iverson, 2013; McCrory et al., 2008; Weil, Ivey, & Karelina, 2023). By identifying when specific pathways have or have not begun to recover, this framework may help prevent premature return during periods of ongoing neural vulnerability (Griesbach et al., 2012; Thomas et al., 2015) and enable more targeted, biologically timed interventions for rehabilitation.

The present findings challenge the traditional view that reduced FA in TBI straightforwardly reflects white matter damage. FA has long been considered a marker of “white matter integrity” (Leow et al., 2009, Shenton et al., 2012, Kochunov et al., 2012, 2007, Kraus et al., 2007, Abdullah et al., 2022), with lower FA in TBI patients compared to healthy controls often interpreted as evidence of structural deterioration (Wallace, Mathias, & Ward, 2018, Hulkower et al., 2013). However, our results show that FA declines before shifting direction over a longer period than expected if it only reflected immediate or irreversible damage. If FA were solely a marker of structural deterioration, its initial magnitude of change would scale with the severity of the insult, but not necessarily influence how long these changes persist. Within this framework, more affected tracts would be expected to show steeper FA reductions early on, but without considering other microstructural processes at play, these changes would be expected to either plateau or continue declining monotonically (e.g., due to Wallerian degeneration; Bendlin et al., 2008, Edlow et al., 2016, Harris et al., 2016, Lindsey et al., 2023). Instead, we observed that tracts exhibiting larger FA changes also showed later inflection points (Fig 2), suggesting that white matter alterations unfold over an extended period, following a trajectory that is not easily explained by passive degeneration alone. More strikingly, rather than signaling ongoing deterioration, these extended FA changes were associated with improved cognitive and emotional outcomes (Fig 3, S5, Table 2). This observation is difficult to reconcile with the idea that FA simply reflects a breakdown in structural integrity. Instead, our findings suggest that FA may also capture dynamic, adaptive processes that influence long-term structural changes.

Ultimately, the conventional framework for interpreting FA in TBI appears incomplete. These findings underscore the need for a more nuanced understanding of FA's role in brain injury, one that accounts for its evolving relationship with functional recovery over time.

An improved interpretation of FA changes is enabled by our complimentary use of DBSI measures. A fundamental challenge in interpreting DTI metrics is that measures like FA can be influenced by multiple physiological processes (Figley et al., 2022). FA stabilization might mask ongoing axonal repair or degeneration (Pierpaoli et al., 2001). Here, we observed that sharp FA reductions immediately after TBI were accompanied by concurrent waves of fluid shifts and cellular remodeling (Fig 4).

The initial TBI insult usually involves rapid acceleration and shear forces that mechanically stretch and compact axons (Chiang et al., 2014; Wang et al., 2017). This transient reshaping of axons allows water diffusion to become more streamlined along surviving fibers, producing a short-lived spike in the fiber ratio. Subsequently, in the first few weeks after TBI, blood–brain barrier breakdown floods the space between cells, driving the hindered-water fraction upward (Wang et al., 2019a).

As microstructural damage mounts, endogenous microglia migrate to clear affected axonal fragments (Mckee & Daneshvar, 2015; Ramlackhansingh et al., 2011). With fewer intact fibers and glial processes in each voxel, the cellularity ratio falls. Although inflammatory "first-responder" cells—namely, leukocytes and reactive astrocytes—also begin to infiltrate, their numbers are small compared to the massive tissue loss. Thus, in this early phase, net cell loss outweighs any swelling (Burda & Sofroniew, 2014). Concomitantly, microvascular constriction, tissue compaction, axonal swelling (Mckee & Daneshvar, 2015) and the initial trickle of inflammatory cells into the interstitial space restrict free water diffusion.

Later, processes associated with acute cleanup taper, and reactive gliosis ramps up: proliferating astrocytes and microglia refill the interstitial gaps, causing the cellularity ratio to rebound (Burda & Sofroniew, 2014). Removal of debris and easing of compaction then frees up extracellular pathways, allowing the free-water fraction to recover, even as edema (hindered ratio) remains elevated. Persistent low perfusion throughout the recovery timeframe suggests ongoing vascular remodeling rather than a true return to baseline (Wang et al., 2019b). Together, these five trajectories sketch a picture of injury → inflammation → cleanup → partial reorganization → chronic remodeling. This timeframe argues for therapeutic windows that extend well beyond the acute phase, such that anti-edema or anti-inflammatory interventions could modulate free-water and hindered signals in the early weeks of the injury, while neuroprotective or pro-remyelination approaches may be most effective during the later gliosis/remodeling phase.

By studying the process of recovery from TBI within rather than across individuals, the present work may more clearly identify biological mechanisms linked

with recovery from TBI—a fundamentally within-individual process—than classic cross-individual, group-average studies. There is growing recognition that results obtained from intra-individual human studies may not be appropriate to infer effects occurring within individuals (Fisher et al. 2018). This so-called “ecological fallacy” (Robinson, 2009, Schwartz, 1994) is a particular concern in human neuroscience (Cragg et al., 2019) and results from issues such as Simpson’s paradox (Blyth, 1972, Kievit et al., 2013, Wagner, 1982), in which within-individual effects can be masked or even appear to reverse direction in cross-individual analyses (see Mattoni et al., 2025 for further discussion). Given the expected cross-individual spatial variability of injury and nonlinear temporal dynamics of recovery, TBI may be a condition in which the ecological fallacy is particularly problematic. Thus, precision imaging approaches studying within-individual effects, such as the one employed here, will be needed for effective clinical translation of DTI measures in TBI (Gratton et al., 2020; Kraus et al., 2023; Laumann et al., 2023; Mattoni et al., 2025).

Ultimately, this work integrates dense longitudinal sampling, advanced statistical modeling, and DBSI to disentangle the complex trajectory of white matter recovery after TBI. By identifying turning points and linking structural changes to symptom resolution, we lay the foundation for time-sensitive, biologically grounded interventions. Clinical guidelines should evolve to incorporate these neurobiological markers, shifting from symptom-based heuristics to precision, biomarker-driven care that optimizes recovery outcomes in TBI.

Methods

1. Participant and Study Characteristics

The participant with TBI identified as a 21yo female with right temporal subdural hematoma (11x8mm) from a motor vehicle collision (MVC; Glascow Coma Scale=15; Teasdale & Jennett, 1974). On arrival at the hospital, she reported a headache but denied nausea, vomiting, new weakness, numbness, or tingling in her extremities. The control participant identified as a 24yo male with no history of neurological or psychiatric conditions.

Both participants underwent weekly MRI scans and behavioral assessments for 27 weeks (~6 months), beginning two weeks after hospital admission for the participant with TBI, followed by an MRI scan and behavioral assessment at their 1-year timepoint. All assessments took place at the Washington University School of Medicine, with Institutional Review Board approval. Both participants provided informed consent for all aspects of the study.

2. Magnetic Resonance Imaging (MRI) Acquisition

Neuroimaging data were acquired using a 3T Siemens Prisma scanner with a 64-channel head coil. Each 45-minute session included the acquisition of 4 types of images: (1) a T1-weighted MP-RAGE (sagittal, 224 slices, TE = 3.74 ms, TR = 2400 ms, flip angle = 8°, 0.8 mm isotropic); (2) a T2-weighted image (sagittal, 224 slices, TE = 479 ms, TR = 3200 ms, flip angle = 120°, 0.8 mm isotropic); (3) a field-map scan (three spin-echo image pairs) for dMRI distortion correction, and (4) a diffusion-weighted imaging (DWI) scan (single-shot echo planar, axial, 75 slices, TE = 83 ms, TR = 3500 ms, 2 mm isotropic, four shells: b-values 250, 500, 1000, and 1500 s/mm², 96 encoding directions). Real-time monitoring was implemented using the Framewise Integrated Real-Time MRI Monitoring (FIRMM) system (Dosenbach et al., 2017), which provided immediate motion feedback to minimize artifacts. All sessions were included based on FIRMM-generated motion quality scores.

3. Preprocessing Pipeline

3.1. T1 & T2-Weighted Images: Workflow: *FSL FAST → Cross Registration → Mean Image Generation → Atlas Registration → FreeSurfer Surface Reconstruction.*

For each subject, FSL FAST was applied to each of the T1- and T2-weighted images to standardize tissue contrast and segmentation (Zhang et al., 2001). All 27 T1 images were linearly cross registered to each other and averaged across sessions to create a mean T1 image using 4dfp tools (https://readthedocs.org/projects/4dfp/); this procedure was then repeated for the T2 images. The mean T1 image was then linearly registered to MNI atlas space using 4dfp tools. The mean T2 image was linearly registered to the mean T1 image and through to MNI space. Finally, both the mean T1-weighted image and the mean T2-weighted image were processed through the

FreeSurfer pipeline (version 7.0) to parcellate cortex, subcortical structures, and white matter.

3.2. Diffusion-Weighted Images (DWI): Workflow: *Eddy Correction & Topup → Motion Correction → DTI Measure Computation → Atlas Registration*

For each session FSL's Eddy correction and Topup was first applied to the DWI scan, using that session's field map scans, to correct for distortions caused by eddy currents and MR field distortions (Smith et al., 2004; Andersson & Sotiropoulos, 2016). Second, volumes with framewise displacement >0.5 mm were removed (Baum et al., 2018). Third, the undistorted B0 volume was extracted and linearly registered to the individual's mean T2-weighted image, and through to MNI space using the T2->MNI registration computed above. Finally, voxelwise diffusion tensors were modeled and DTI metrics were computed from the session using FSL's DTIFIT. These metrics included (1) *Fractional Anisotropy* (FA), estimated by the extent of directional (anisotropic) water diffusion in each voxel; (2) *Axial Diffusivity* (AD), estimated by the extent of water diffusion along the primary (longest) tensor axis of each voxel; (3) Radial Diffusivity (RD), estimated by the extent of water diffusion perpendicular to the primary axis each voxel; and (4) Mean Diffusivity (MD), estimated as the average water diffusion in all axes of each voxel. These metric maps, as well as the original distortion-corrected DWI images, were registered to MNI space using the DWI->MNI registration.

4. Processing Pipeline

4.1. Fiber Tract Definition and DTI Metric extraction: Workflow: *Estimate Tract Probabilities → Integrate with Participant's DWI Data → Model Fiber Orientations (bedpostX) → Reconstruct Tracts in Participant's Native Space → Register to MNI space → Extract FA, RD, MD, and AD Measures*

First, prior probabilities were estimated by combining a white matter atlas with FreeSurfer-derived cortical and subcortical segmentations (Section 3.1.), determining the likelihood of each tract passing through or near specific anatomical regions. Second, these priors were combined with the participant's MNI-space diffusion-weighted data to refine tract estimates. Third, FSL's bedpostX tool was used to fit a ball-and-stick diffusion model, allowing for the representation of up to two distinct fiber orientations per voxel. Fourth, using the estimated fiber orientation vectors and anatomical priors, the TRACULA tool (TRActs Constrained by UnderLying Anatomy; Yendiki et al., 2011) reconstructed each white matter tract, preserving individual anatomical variation and ensuring longitudinal consistency. The final output consisted of probabilistic tract maps representing the most likely trajectories of each of 18 major white matter pathways. These pathways included forceps major, forceps minor, left and right corticospinal tract (CST), inferior longitudinal fasciculus (ILF), uncinate fasciculus (UNC), anterior thalamic radiation (ATR), cingulum-cingulate gyrus bundle (CCG), cingulum-angular bundle (CAB), and superior longitudinal fasciculus (SLF; temporal and parietal branches). Fifth, a streamline threshold of three was applied to the tract maps, to retain only voxels with

sufficient probabilistic support for belonging to a given tract. This thresholding process produced individual-specific MNI-space masks for each tract. Finally, we computed mean diffusion metrics (FA, AD, RD, and MD) within each tract mask for every imaging session.

4.2. Diffusion Based Spectrum Imaging (DBSI; Wang et al., 2015, 2014, 2011**):**

Workflow: *Raw DWI Signal → Multi-Compartment Model Fitting → Regularized Non-Negative Inversion → Extract Diffusion Metrics (Fiber Ratio, Cellularity Ratio, Free Water Ratio, Hindered Ratio, and Perfusion Ratio)*

First, the direction-specific diffusion MRI signals within each voxel of the undistorted MNI-space DWI data was decomposed using a multi-compartment model that accounts for different cerebral anatomical and pathological components, including anisotropic white and gray matter fibers, inflammatory cells, extracellular water (edema), and CSF. Second, a regularized nonnegative least-squares analysis was applied to prevent overfitting, incorporating prior knowledge about signal intensities and energy constraints. Third, the model estimated key diffusion parameters, including anisotropic signal fractions, which reflect white matter integrity, axial and radial diffusivity, which assess water movement along and across white matter fibers to infer microstructural health, and an isotropic diffusion spectrum, which quantifies cellular and extracellular properties. For tract-specific extraction, thresholded white matter masks from TRACULA's MNI-registered tract maps (Section 4.1) were applied to the DBSI-derived parameter maps. This step ensured that diffusion measures were computed only from voxels with a high probability of belonging to a given white matter tract, reducing contamination from surrounding tissue or CSF. Subsequently, mean DBSI metrics were extracted for each tract at every imaging session: (1) *fiber ratio*, quantifying the proportion of intact white matter fibers, (2) *cellularity ratio*, quantifying the extent of restricted diffusion linked to immune cell infiltration, (3) *free water ratio*, quantifying extracellular water content indicative of edema, (4) *hindered ratio*, quantifying intracellular water changes due to swelling or cell infiltration, and, (5) *perfusion ratio*, quantifying vascular blood flow, which may vary with inflammation.

5. Cognitive and Emotion Assessments

5.1. Number-Symbol Coding Task

This task simplifies the traditional Symbol Digit Modalities Test (SDMT; Smith 1973; Jaeger 2018) by reducing the number of symbol-digit pairs from nine to three, where each digit (1, 2, or 3) is associated with three different symbols (see Figure 2). Participants are required to identify the correct digit for a given target symbol, providing a measure of processing speed, pattern recognition, and cognitive flexibility while minimizing cognitive load. A digitized version of the task was used in this study, and prior research has demonstrated high correlations between the digital and traditional paper-and-pencil versions (Pham et al., 2021). This task has shown high sensitivity to

detecting changes following neurological injury (Jaeger et al., 2018, Galvin et al., 2020), making it a valuable tool for longitudinal cognitive assessment. Moreover, its construct validity ensures that performance is not confounded by anxiety or depression (Jaeger et al., 2018; Table 2), allowing it to be reliably interpreted as a measure of cognitive recovery following TBI.

5.2. Beck Anxiety Inventory (**BAI**; Beck et al., 1993)

The BAI is a 21-item self-report measure designed to assess the severity of anxiety symptoms over the past week. Participants rate the presence of physical symptoms (e.g., *"Numbness or tingling"*) and cognitive symptoms (e.g., *"Fear of losing control"*) on a 4-point Likert scale, with higher scores indicating greater symptom severity. The BAI demonstrates high specificity for anxiety symptoms and effectively differentiates anxiety from depressive symptomatology.

5.3. Beck Depression Inventory (**BDI**; Beck et al., 1996)

The BDI is a 21-item self-report measure designed to assess the severity of depressive symptoms over the past two weeks (modified to a one-week timeframe for this study). Participants rate the presence of physical symptoms (e.g., *"Tiredness or fatigue"*), affective symptoms (e.g., *"Sadness"*), behavioral symptoms (e.g., *"Loss of interest in activities"*), and cognitive symptoms (e.g., *"Self-criticism"*) on a 4-point Likert scale, with higher scores reflecting greater symptom severity. The BDI demonstrates high specificity for depressive symptoms and effectively distinguishes depression from anxiety-related symptomatology.

6. Analyses

All statistical analyses were conducted in R (4.4.1, studio version:2024.12.0+467).

6.1. Modeling Trajectories of DTI and DBSI Metrics over Time

To characterize white matter changes over the 27 imaging sessions, linear and quadratic mixed-effects models were fitted to individual DTI and DBSI metrics for each participant to capture potential nonlinear recovery patterns. This modeling framework allowed us to capture general patterns of change in each DTI/DBSI metric over time (e.g., evaluating how weeks since TBI^2 relates to FA values across all brain tracts; fixed effect), while also accounting for the possibility that different brain tracts have different starting values (i.e., random effect of tract-intercept) and distinct rates of change over time (i.e., random effect of slope; R package, lme4; Bates et al., 2015).

Following best practices in confirmatory hypothesis testing (Barr et al., 2013), we specified a maximal random effects structure, incorporating the most complex model justified by the data to account for variability and enhance generalizability (i.e., starting out with a model that incorporated both random intercept and for tract variation over time). These models were defined as follows:

Linear model

$$White\ Matter\ Metric \sim Weeks\ Since\ TBI + Head\ Motion + (1 + Weeks\ Since\ TBI\ |Tract)$$

$$White\ Matter\ Metric \sim Weeks\ Since\ TBI + Head\ Motion + (1 + Weeks\ Since\ TBI\ |Tract)$$

Quadratic model

$$White\ Matter\ Metric \sim Weeks\ Since\ TBI + Weeks\ Since\ TBI^2 + Head\ Motion + (1 + Weeks\ Since\ TBI\ |Tract)$$

where:

$Weeks\ Since\ TBI$ captures the main effect of time ($Weeks\ Since\ Enrollment$ for control participant)

$Weeks\ Since\ TBI^2$ accounts for potential nonlinear changes ($Weeks\ Since\ Enrollment^2$ for control participant),

$Head\ Motion$ controls for participant movement in the scanner, which could introduce noise in the diffusion signal, and
the notation $(1 + Weeks\ Since\ TBI\ |Tract)$ (or $(1 + Weeks\ Since\ Enrollment\ |Tract)$ for the control participant) represents random intercepts and slopes, allowing each tract to have its own baseline diffusion/DBSI measure (random intercept) and its own rate of change over time (random slope).

Model fit was evaluated using Akaike Information Criterion (AIC) and ANOVA model comparisons (Table 1). To ensure model stability, all analyses were bootstrapped 1000 times, and models were only accepted if they converged across all iterations. We parsed the separate contributions of fixed effects ($R^2_{marginal}$) and combined fixed and random effects ($R^2_{conditional}$) using the MumIn package in R (Bartoń K, 2024; Table 1).

Results indicated that FA and RD followed a quadratic trajectory over time (i.e., modeling weeks since TBI^2 as a fixed effect) with random intercept and slope for tracts (random effects), while MD followed a quadratic trajectory with only random intercept for tracts. In contrast to these quadratic fits, AD best fit a linear mixed-effects model (fixed effect of weeks since TBI) with only random intercept for tracts, Table 1; Result [1]). Model fits for DBSI measures are summarized in Table 1 (Result [4]).

To map these effects onto individual tracts, we estimated adjusted R^2 values for each tract, modeling tract-wise quadratic effects for FA, RD, and MD and tract-wise linear effects for AD. These R^2 values were projected onto MNI-registered tract maps (Result [1]).

Linear model (tract-wise)

$$DTI\ Metric_{Tract} \sim Weeks\ Since\ TBI_{Tract} + \ Head\ Motion_{Tract}$$

Quadratic model (tract-wise)

$$DTI\ Metric_{Tract} \sim \ Weeks\ Since\ TBI_{Tract} + \ Weeks\ Since\ TBI_{Tract}{}^{2} \ + \ Head\ Motion_{Tract}$$

These models were extended to project recovery trajectories up to the one-year timepoint, providing a broader view of long-term white matter changes (Result [4]).

6.2. Modeling Trajectories of Cognitive and Emotion Outcomes and Contributions of White Matter

We modeled the trajectories of cognitive performance (reaction time on accurate trials of the Number-Symbol Coding task) and mean scores on the BAI (anxiety) and BDI (depression) over time for both participants (Result [3]).

To determine whether DTI changes mediated cognitive recovery over time, we implemented a quadratic mediation framework (Preacher & Hayes, 2008). This approach tests whether DTI metrics (FA, RD, MD, AD) mediate improvements in cognitive task performance over weeks since TBI (or Weeks since Enrollment for the control participant). For each participant and tract, we specifically modeled the following:

Mediator Path Model

$$DTI\ Metric = \ \beta_0 + \ \beta_1\ (Weeks\ Since\ TBI) + \ \beta_2\ (Weeks\ Since\ TBI^2) + \ \beta_3\ (Head\ Motion) + \ \varepsilon$$

This model estimates how Weeks since TBI (or Weeks since Enrollment for the control participant) affects the DTI metric (the mediator), with β_1 capturing this effect.

Outcome Path Model

$$Reaction\ time\ on\ NumSym = \ \gamma_0 + \ \gamma_1\ (Weeks\ Since\ TBI) + \ \gamma_2\ (Weeks\ Since\ TBI^2) + \ \gamma_3\ (DTI\ Metric) + \zeta$$

This model tests whether variation in DTI metrics predicts cognitive processing speed —as indexed by reaction time on the Number-Symbol Coding task—while controlling for time since TBI (or enrollment). The coefficient γ_3 captures the effect of DTI changes on reaction time, while γ_1 and γ_2 account for the linear and quadratic effects of Weeks since TBI (or enrollment), respectively.

Indirect & Total Effects:

The indirect effect, which quantifies mediation, is computed as:

$$\delta = \beta_1 . \gamma_3 + \beta_2 . \gamma_3$$

This equation captures the mediation of both the linear and quadratic components of Weeks since TBI (or enrollment) on reaction time via changes in DTI metrics.

The total effect of Weeks since TBI (or enrollment) on cognitive performance is computed as:

$$\tau = \delta + \gamma_1 + \gamma_2$$

where:

τ represents the total effect of time since injury (or enrollment) on cognition,

δ is the indirect effect mediated by DTI changes, and,

$\gamma_1 \; and \; \gamma_2$ are the direct unmediated effects of time on reaction time, capturing both the linear and quadratic influence.

Mediation effects were estimated using bootstrapped confidence intervals (5000 simulations; Preacher & Hayes, 2008) to account for non-normality. Proportion mediated was computed as $\frac{\delta}{\tau}$ x 100, indicating the percentage of the total effect of time mediated by white matter changes. Mediation effects were classified as full, partial, or none based on the significance of indirect and direct effects (Table 2).

This approach addresses limitations of traditional mediation models (Baron & Kenny, 1986) by allowing for causal inference under weaker assumptions. The Preacher & Hayes framework, implemented via the mediation package in R (Tingley et al., 2014), explicitly quantifies indirect and direct effects, provides robust uncertainty estimates, and accommodates nonlinear relationships, making it particularly well-suited for modeling complex neurobiological recovery trajectories.

For comparison, a simpler linear mediation model was also conducted (Table 2), wherein all DTI metrics and reaction time were modeled as linear functions of weeks since TBI (or weeks since enrollment). In this instance:

Mediator Path Model

$$DTI \; Metric = \beta_0 + \beta_1 \; (Weeks \; Since \; TBI) + \beta_2 (Head \; Motion) + \varepsilon$$

Outcome Path Model

$$Reaction \; time \; on \; NumSym = \gamma_0 + \gamma_1 \; (Weeks \; Since \; TBI) + \gamma_2 \; (DTI \; Metric) + \zeta$$

Indirect & Total Effects:

The indirect effect is computed as:

$$\delta = \beta_1 . \gamma_2$$

The total effect of weeks since TBI on cognitive performance is computed as:

$\tau = \delta + \gamma_1$

where:

τ represents the total effect of time since injury on cognition,

δ is the indirect effect mediated by DTI changes, and,

γ_1 is the direct unmediated effects of time on reaction time, capturing both the linear and quadratic influence.

Both quadratic and linear mediation models were replicated for emotional outcomes, with the same mediation path models and indirect and total effects calculations (Table 2). The outcome path model was defined as:

$Mean\ Anxiety\ [Depression]\ Score = \gamma_0 + \gamma_1\ (Weeks\ Since\ TBI) + \gamma_2\ (Weeks\ Since\ TBI^2) + \gamma_3\ (DTI\ Metric) + \zeta$ for the quadratic effect, and as

$Mean\ Anxiety\ [Depression]\ Score = \gamma_0 + \gamma_1\ (Weeks\ Since\ TBI) + \gamma_2\ (DTI\ Metric) + \zeta$ for the linear effect.

6.3. Assessing Tract-Specific Recovery at 1-Year Post-Injury

To evaluate whether white matter recovery was complete at the tract level, we modeled tract-specific diffusion trajectories using quadratic functions fit to data from the first six months post-injury. For each tract, we estimated the predicted timepoint at which the diffusion metric—either fractional anisotropy (FA) or radial diffusivity (RD)—would return to its early post-injury baseline (Week 1). Recovery was defined as a return to this individualized baseline, reflecting the assumption that Week 1 values provide a tract-specific anchor for post-injury status prior to subsequent remodeling.

Quadratic models were fit separately for each tract using the equation:

$DTI\ Metric = \beta_0 + \beta_1\ (Weeks\ Since\ TBI) + \beta_2(Head\ Motion) + \varepsilon$

Predicted return-to-baseline timepoints were calculated as:

$$t_{return} = 2t_{vertex} - t_0,$$

$where\ t_{vertex}\ is\ the\ vertex\ of\ the\ quadratic\ (turning\ point)$
$where\ t_0 = 1\ (week\ 1)$

The expected diffusion value at $t_{return}$was then computed along with 95% confidence intervals using the delta method. To assess recovery status at one year, we compared the observed 1-year diffusion metric for each tract (Week 51) to the predicted return-to-baseline value. Tracts were classified as “Recovered” if the 1-year value fell within the 95% confidence interval of the predicted return, and “Not Recovered” if it fell outside this range.

References

Abdullah, A. N., Ahmad, A. H., Zakaria, R., Tamam, S., Abd Hamid, A. I., Chai, W. J., ... & Abdullah, J. M. (2022). Disruption of white matter integrity and its relationship with cognitive function in non-severe traumatic brain injury. *Frontiers in Neurology*, *13*, 1011304.

Amyot, F., Arciniegas, D. B., Brazaitis, M. P., Curley, K. C., Diaz-Arrastia, R., Gandjbakhche, A., ... & Stocker, D. (2015). A review of the effectiveness of neuroimaging modalities for the detection of traumatic brain injury. *Journal of neurotrauma*, *32*(22), 1693-1721.

Andersson, J. L., & Sotiropoulos, S. N. (2016). An integrated approach to correction for off-resonance effects and subject movement in diffusion MR imaging. *Neuroimage*, *125*, 1063-1078.

Armstrong, R. C., Mierzwa, A. J., Marion, C. M., & Sullivan, G. M. (2016). White matter involvement after TBI: Clues to axon and myelin repair capacity. *Experimental neurology*, *275*, 328-333.

Barr, D. J., Levy, R., Scheepers, C., & Tily, H. J. (2013). Random effects structure for confirmatory hypothesis testing: Keep it maximal. *Journal of memory and language*, *68*(3), 255-278.

Baron, R. M., & Kenny, D. A. (1986). The moderator–mediator variable distinction in social psychological research: Conceptual, strategic, and statistical considerations. *Journal of personality and social psychology*, *51*(6), 1173.

Bartels, C., Wegrzyn, M., Wiedl, A., Ackermann, V., & Ehrenreich, H. (2010). Practice effects in healthy adults: a longitudinal study on frequent repetitive cognitive testing. *BMC neuroscience*, *11*, 1-12.

Bates, D., Mächler, M., Bolker, B., & Walker, S. (2015). Fitting linear mixed-effects models using lme4. *Journal of statistical software*, *67*, 1-48.

Bartoń K (2024). *MuMIn: Multi-Model Inference*. R package version 1.48.4, https://CRAN.R-project.org/package=MuMIn.

Beck, A. T., Epstein, N., Brown, G., & Steer, R. (1993). Beck anxiety inventory. *Journal of consulting and clinical psychology*.

Beck, A. T., Steer, R. A., & Brown, G. K. (1996). Beck depression inventory.

Bendlin, B. B., Ries, M. L., Lazar, M., Alexander, A. L., Dempsey, R. J., Rowley, H. A., ... & Johnson, S. C. (2008). Longitudinal changes in patients with traumatic brain injury assessed with diffusion-tensor and volumetric imaging. *Neuroimage*, *42*(2), 503-514.

Braga, R. M., & Buckner, R. L. (2017). Parallel interdigitated distributed networks within the individual estimated by intrinsic functional connectivity. *Neuron*, *95*(2), 457-471.

Brickman, A. M., Zimmerman, M. E., Paul, R. H., Grieve, S. M., Tate, D. F., Cohen, R. A., ... & Gordon, E. (2006). Regional white matter and neuropsychological functioning across the adult lifespan. *Biological psychiatry*, *60*(5), 444-453.

Baum, G. L., Roalf, D. R., Cook, P. A., Ciric, R., Rosen, A. F., Xia, C., ... & Satterthwaite, T. D. (2018). The impact of in-scanner head motion on structural connectivity derived from diffusion MRI. *Neuroimage*, *173*, 275-286.

Blyth, C. R. (1972). On Simpson's paradox and the sure-thing principle. *Journal of the American Statistical Association*, *67*(338), 364-366.

Bumham, K. P., & Anderson, D. R. (2002). Model selection and multimodel inference: a practical information-theoretic approach. *Spnnger-Veflag, New York, New York*.

Carroll, L., Cassidy, J. D., Peloso, P., Borg, J., Von Holst, H., Holm, L., ... & Pépin, M. (2004). Prognosis for mild traumatic brain injury: results of the WHO Collaborating Centre Task Force on Mild Traumatic Brain Injury. *Journal of rehabilitation medicine*, 36(0), 84-105.

Catani, M., Dell'Acqua, F., Bizzi, A., Forkel, S. J., Williams, S. C., Simmons, A., ... & de Schotten, M. T. (2012). Beyond cortical localization in clinico-anatomical correlation. *cortex*, 48(10), 1262-1287.

Chiang, C. W., Wang, Y., Sun, P., Lin, T. H., Trinkaus, K., Cross, A. H., & Song, S. K. (2014). Quantifying white matter tract diffusion parameters in the presence of increased extra-fiber cellularity and vasogenic edema. *Neuroimage*, *101*, 310-319.

Chiou, K. S., Jiang, T., Chiaravalloti, N., Hoptman, M. J., DeLuca, J., & Genova, H. (2019). Longitudinal examination of the relationship between changes in white matter organization and cognitive outcome in chronic TBI. *Brain injury*, 33(7), 846-853.

Cook, J. A., Ramsaya, C. R., & Fayers, P. (2004). Statistical evaluation of learning curve effects in surgical trials. *Clinical Trials*, *1*(5), 421-427.

Cragg, J. J., Kramer, J. L., Borisoff, J. F., Patrick, D. M., & Ramer, M. S. (2019). Ecological fallacy as a novel risk factor for poor translation in neuroscience research: A systematic review and simulation study. *European journal of clinical investigation*, *49*(2), e13045.

Dosenbach, N. U., Koller, J. M., Earl, E. A., Miranda-Dominguez, O., Klein, R. L., Van, A. N., ... & Fair, D. A. (2017). Real-time motion analytics during brain MRI improve data quality and reduce costs. *Neuroimage*, *161*, 80-93.

Edlow, B. L., Copen, W. A., Izzy, S., Bakhadirov, K., van der Kouwe, A., Glenn, M. B., ... & Wu, O. (2016). Diffusion tensor imaging in acute-to-subacute traumatic brain injury: a longitudinal analysis. *BMC neurology*, *16*, 1-11.

Eierud, C., Craddock, R. C., Fletcher, S., Aulakh, M., King-Casas, B., Kuehl, D., & LaConte, S. M. (2014). Neuroimaging after mild traumatic brain injury: review and meta-analysis. *NeuroImage: Clinical*, 4, 283-294.

Figley, C. R., Uddin, M. N., Wong, K., Kornelsen, J., Puig, J., & Figley, T. D. (2022). Potential pitfalls of using fractional anisotropy, axial diffusivity, and radial diffusivity as biomarkers of cerebral white matter microstructure. *Frontiers in Neuroscience*, *15*, 799576.

Filley, C. (2012). The behavioral neurology of white matter. Oxford University Press.

Fisher, A. J., Medaglia, J. D., & Jeronimus, B. F. (2018). Lack of group-to-individual generalizability is a threat to human subjects research. *Proceedings of the National Academy of Sciences*, *115*(27), E6106-E6115.

Forkel, S. J., Friedrich, P., Thiebaut de Schotten, M., & Howells, H. (2022). White matter variability, cognition, and disorders: a systematic review. *Brain Structure and Function*, 1-16.

Frencham, K. A., Fox, A. M., & Maybery, M. T. (2005). Neuropsychological studies of mild traumatic brain injury: A meta-analytic review of research since 1995. *Journal of clinical and experimental neuropsychology*, 27(3), 334-351.

Galvin, J. E., Tolea, M. I., Moore, C., & Chrisphonte, S. (2020). The Number Symbol Coding Task: A brief measure of executive function to detect dementia and cognitive impairment. *PLoS One*, *15*(11), e0242233.

Gennarelli, T. A., Thibault, L. E., Adams, J. H., Graham, D. I., Thompson, C. J., & Marcincin, R. P. (1982). Diffuse axonal injury and traumatic coma in the primate. Annals of Neurology: Official Journal of the American Neurological Association and the Child Neurology Society, 12(6), 564-574.

Gratton, C., Kraus, B. T., Greene, D. J., Gordon, E. M., Laumann, T. O., Nelson, S. M., ... & Petersen, S. E. (2020). Defining individual-specific functional neuroanatomy for precision psychiatry. *Biological psychiatry*, *88*(1), 28-39.

Gratton, C., Nelson, S. M., & Gordon, E. M. (2022). Brain-behavior correlations: Two paths toward reliability. *Neuron*, *110*(9), 1446-1449.

Gordon, E. M., Laumann, T. O., Gilmore, A. W., Newbold, D. J., Greene, D. J., Berg, J. J., ... & Dosenbach, N. U. (2017). Precision functional mapping of individual human brains. *Neuron*, *95*(4), 791-807.

Gordon, E. M., Chauvin, R. J., Van, A. N., Rajesh, A., Nielsen, A., Newbold, D. J., ... & Dosenbach, N. U. (2023). A somato-cognitive action network alternates with effector regions in motor cortex. *Nature*, *617*(7960), 351-359.

Gyebnár, G., Szabó, Á., Sirály, E., Fodor, Z., Sákovics, A., Salacz, P., ... & Csukly, G. (2018). What can DTI tell about early cognitive impairment?–Differentiation between MCI subtypes and healthy controls by diffusion tensor imaging. *Psychiatry Research: Neuroimaging*, *272*, 46-57.

Han, D. H., Renshaw, P. F., Dager, S. R., Chung, A., Hwang, J., Daniels, M. A., ... & Lyoo, I. K. (2008). Altered cingulate white matter connectivity in panic disorder patients. *Journal of psychiatric research*, *42*(5), 399-407.

Harris, N. G., Verley, D. R., Gutman, B. A., & Sutton, R. L. (2016). Bi-directional changes in fractional anisotropy after experiment TBI: Disorganization and reorganization? *Neuroimage*, *133*, 129-143.

Holm, S. P., Wolfer, A. M., Pointeau, G. H., Lipsmeier, F., & Lindemann, M. (2022). Practice effects in performance outcome measures in patients living with neurologic disorders–A systematic review. *Heliyon*, *8*(8).

Hulkower, M. B., Poliak, D. B., Rosenbaum, S. B., Zimmerman, M. E., & Lipton, M. L. (2013). A decade of DTI in traumatic brain injury: 10 years and 100 articles later. *American Journal of Neuroradiology*, 34(11), 2064-2074.

Jaeger, J. (2018). Digit symbol substitution test: the case for sensitivity over specificity in neuropsychological testing. *Journal of clinical psychopharmacology*, *38*(5), 513-519.

Jiang, M., Li, C. L., Zhang, S. Y., Gao, X., & Yang, X. F. (2023). The incidence of brain trauma caused by road injuries: Results from the Global Burden of Disease Study 2019. *Injury*, *54*(12), 110984.

Karlsen, R. H., Einarsen, C., Moe, H. K., Håberg, A. K., Vik, A., Skandsen, T., & Eikenes, L. (2019). Diffusion kurtosis imaging in mild traumatic brain injury and postconcussional syndrome. *Journal of neuroscience research*, *97*(5), 568-581.

Kievit, R. A., Frankenhuis, W. E., Waldorp, L. J., & Borsboom, D. (2013). Simpson's paradox in psychological science: a practical guide. *Frontiers in psychology*, *4*, 513.

Kim, E., Yoo, R. E., Seong, M. Y., & Oh, B. M. (2022). A systematic review and data synthesis of longitudinal changes in white matter integrity after mild traumatic brain injury assessed by diffusion tensor imaging in adults. *European Journal of Radiology*, *147*, 110117.

Kochunov, P., Thompson, P. M., Lancaster, J. L., Bartzokis, G., Smith, S., Coyle, T., ... & Fox, P. T. (2007). Relationship between white matter fractional anisotropy and other indices of cerebral health in normal aging: tract-based spatial statistics study of aging. *Neuroimage*, *35*(2), 478-487.

Kochunov, P., Williamson, D. E., Lancaster, J., Fox, P., Cornell, J., Blangero, J., & Glahn, D. C. (2012). Fractional anisotropy of water diffusion in cerebral white matter across the lifespan. *Neurobiology of aging*, *33*(1), 9-20.

Kraus, M. F., Susmaras, T., Caughlin, B. P., Walker, C. J., Sweeney, J. A., & Little, D. M. (2007). White matter integrity and cognition in chronic traumatic brain injury: a diffusion tensor imaging study. *Brain*, *130*(10), 2508-2519.

Kraus, B., Zinbarg, R., Braga, R. M., Nusslock, R., Mittal, V. A., & Gratton, C. (2023). Insights from personalized models of brain and behavior for identifying biomarkers in psychiatry. *Neuroscience & Biobehavioral Reviews*, *152*, 105259.

Laumann, T. O., Gordon, E. M., Adeyemo, B., Snyder, A. Z., Joo, S. J., Chen, M. Y., ... & Petersen, S. E. (2015). Functional system and areal organization of a highly sampled individual human brain. *Neuron*, *87*(3), 657-670.

Laumann, T., Snyder, A., Brown, H., Gott, B., Gordon, E., Barch, D., ... & Conway, C. (2023, December). Feasibility of Precision Functional Mapping in Treatment-Resistant Depression. *Neuropsychopharmacology*, 48, 287-288.

Lindsey, H. M., Hodges, C. B., Greer, K. M., Wilde, E. A., & Merkley, T. L. (2023). Diffusion-weighted imaging in mild traumatic brain injury: a systematic review of the literature. *Neuropsychology Review*, *33*(1), 42-121.

Ling, J. M., Pena, A., Yeo, R. A., Merideth, F. L., Klimaj, S., Gasparovic, C., & Mayer, A. R. (2012). Biomarkers of increased diffusion anisotropy in semi-acute mild traumatic brain injury: a longitudinal perspective. *Brain*, 135(4), 1281-1292.

Leow, A. D., Zhan, L., Zhu, S., Hageman, N., Chiang, M. C., Barysheva, M., ... & Thompson, P. M. (2009, June). White matter integrity measured by fractional anisotropy correlates poorly with actual individual fiber anisotropy. In *2009 IEEE International Symposium on Biomedical Imaging: From Nano to Macro* (pp. 622-625). IEEE.

Lynch, C. J., Elbau, I. G., Ng, T., Ayaz, A., Zhu, S., Wolk, D., ... & Liston, C. (2024). Frontostriatal salience network expansion in individuals in depression. *Nature*, *633*(8030), 624-633.

Maas, A. I., Menon, D. K., Manley, G. T., Abrams, M., Åkerlund, C., Andelic, N., ... & Zemek, R. (2022). Traumatic brain injury: progress and challenges in prevention, clinical care, and research. *The Lancet Neurology*, *21*(11), 1004-1060.

Mattoni, M., Fisher, A. J., Gates, K. M., Chein, J., & Olino, T. M. (2025). Group-to-Individual Generalizability and Individual-Level Inferences in Cognitive Neuroscience. *Neuroscience & Biobehavioral Reviews*, 106024.

Mayer, A. R., Ling, J., Mannell, M. V., Gasparovic, C., Phillips, J. P., Doezema, D., ... & Yeo, R. (2010). A prospective diffusion tensor imaging study in mild traumatic brain injury. *Neurology*, 74(8), 643-650.

Mesaros, S., Rocca, M. A., Kacar, K., Kostic, J., Copetti, M., Stosic-Opincal, T., ... & Filippi, M. (2012). Diffusion tensor MRI tractography and cognitive impairment in multiple sclerosis. *Neurology*, *78*(13), 969-975.

Michon, K. J., Khammash, D., Simmonite, M., Hamlin, A. M., & Polk, T. A. (2022). Person-specific and precision neuroimaging: Current methods and future directions. *NeuroImage*, *263*, 119589.

Murphy, M. L., & Frodl, T. (2011). Meta-analysis of diffusion tensor imaging studies shows altered fractional anisotropy occurring in distinct brain areas in association with depression. *Biology of mood & anxiety disorders*, *1*, 1-12.

Næss-Schmidt, E. T., Blicher, J. U., Eskildsen, S. F., Tietze, A., Hansen, B., Stubbs, P. W., ... & Nielsen, J. F. (2017). Microstructural changes in the thalamus after mild traumatic brain injury: a longitudinal diffusion and mean kurtosis tensor MRI study. *Brain injury*, *31*(2), 230-236.

Nakayama, N., Okumura, A., Shinoda, J., Yasokawa, Y. T., Miwa, K., Yoshimura, S. I., & Iwama, T. (2006). Evidence for white matter disruption in traumatic brain injury without macroscopic lesions. *Journal of Neurology, Neurosurgery & Psychiatry*, 77(7), 850-855.

Narayana, P. A., Yu, X., Hasan, K. M., Wilde, E. A., Levin, H. S., Hunter, J. V., ... & McCarthy, J. J. (2015). Multi-modal MRI of mild traumatic brain injury. *NeuroImage: Clinical*, *7*, 87-97.

Naselaris, T., Allen, E., & Kay, K. (2021). Extensive sampling for complete models of individual brains. *Current Opinion in Behavioral Sciences*, *40*, 45-51.

Newbold, D. J., Laumann, T. O., Hoyt, C. R., Hampton, J. M., Montez, D. F., Raut, R. V., ... & Dosenbach, N. U. (2020). Plasticity and spontaneous activity pulses in disused human brain circuits. *Neuron*, *107*(3), 580-589.

Niogi, S. N., & Mukherjee, P. (2010). Diffusion tensor imaging of mild traumatic brain injury. The *Journal of head trauma rehabilitation*, 25(4), 241-255.

Palacios, E. M., Owen, J. P., Yuh, E. L., Wang, M. B., Vassar, M. J., Ferguson, A. R., ... & Track-TBI Investigators. (2020). The evolution of white matter microstructural changes after mild traumatic brain injury: a longitudinal DTI and NODDI study. *Science advances*, 6(32), eaaz6892.

Pham, L., Harris, T., Varosanec, M., Morgan, V., Kosa, P., & Bielekova, B. (2021). Smartphone-based symbol-digit modalities test reliably captures brain damage in multiple sclerosis. *NPJ digital medicine*, *4*(1), 36.

Pierpaoli, C., Barnett, A., Pajevic, S., Chen, R., Penix, L., Virta, A., & Basser, P. (2001). Water diffusion changes in Wallerian degeneration and their dependence on white matter architecture. *Neuroimage*, *13*(6), 1174-1185.

Preacher, K. J., & Hayes, A. F. (2008). Asymptotic and resampling strategies for assessing and comparing indirect effects in multiple mediator models. *Behavior research methods*, *40*(3), 879-891.

Preziosa, P., Pagani, E., Meani, A., Marchesi, O., Conti, L., Falini, A., ... & Filippi, M. (2023). NODDI, diffusion tensor microstructural abnormalities and atrophy of brain white matter and gray matter contribute to cognitive impairment in multiple sclerosis. *Journal of Neurology*, *270*(2), 810-823.

Pritschet, L., Santander, T., Taylor, C. M., Layher, E., Yu, S., Miller, M. B., ... & Jacobs, E. G. (2020). Functional reorganization of brain networks across the human menstrual cycle. *Neuroimage*, *220*, 117091.

Pritschet, L., Taylor, C. M., Cossio, D., Faskowitz, J., Santander, T., Handwerker, D. A., ... & Jacobs, E. G. (2024). Neuroanatomical changes observed over the course of a human pregnancy. *Nature Neuroscience*, *27*(11), 2253-2260.

Roberts, R. E., Anderson, E. J., & Husain, M. (2013). White matter microstructure and cognitive function. *The Neuroscientist*, 19(1), 8-15.

Robinson, W. S. (2009). Ecological correlations and the behavior of individuals. *International journal of epidemiology*, *38*(2), 337-341.

Rosenbaum, S. B., & Lipton, M. L. (2012). Embracing chaos: the scope and importance of clinical and pathological heterogeneity in mTBI. *Brain imaging and behavior*, *6*, 255-282.

Schmahmann, J. D., Smith, E. E., Eichler, F. S., & Filley, C. M. (2008). Cerebral white matter: neuroanatomy, clinical neurology, and neurobehavioral correlates. *Annals of the New York Academy of Sciences*, *1142*(1), 266-309.

Schretlen, D. J., & Shapiro, A. M. (2003). A quantitative review of the effects of traumatic brain injury on cognitive functioning. *International review of psychiatry*, 15(4), 341-349.

Schwartz, S. (1994). The fallacy of the ecological fallacy: the potential misuse of a concept and the consequences. *American journal of public health*, *84*(5), 819-824.

Sexton, C. E., Mackay, C. E., & Ebmeier, K. P. (2009). A systematic review of diffusion tensor imaging studies in affective disorders. *Biological psychiatry*, *66*(9), 814-823.

Shenton, M. E., Hamoda, H. M., Schneiderman, J. S., Bouix, S., Pasternak, O., Rathi, Y., ... & Zafonte, R. (2012). A review of magnetic resonance imaging and diffusion tensor imaging findings in mild traumatic brain injury. *Brain imaging and behavior*, *6*, 137-192.

Siegel, J. S., Subramanian, S., Perry, D., Kay, B. P., Gordon, E. M., Laumann, T. O., ... & Dosenbach, N. U. (2024). Psilocybin desynchronizes the human brain. *Nature*, *632*(8023), 131-138.

Smith, A. (1973). Symbol digit modalities test. *The clinical neuropsychologist*.

Smith, S. M., Jenkinson, M., Woolrich, M. W., Beckmann, C. F., Behrens, T. E., Johansen-Berg, H., ... & Matthews, P. M. (2004). Advances in functional and structural MR image analysis and implementation as FSL. *Neuroimage*, *23*, S208-S219.

Teasdale, G., & Jennett, B. (1974). *Assessment of coma and impaired consciousness. A Practical Scale Lancet 2: 81–84*.

Tingley, D., Yamamoto, T., Hirose, K., Keele, L., & Imai, K. (2014). Mediation: R package for causal mediation analysis. *Journal of statistical software*, *59*, 1-38.

Wagner, C. H. (1982). Simpson's paradox in real life. *The American Statistician*, *36*(1), 46-48.

Wallace, E. J., Mathias, J. L., & Ward, L. (2018). Diffusion tensor imaging changes following mild, moderate and severe adult traumatic brain injury: a meta-analysis. *Brain imaging and behavior*, *12*, 1607-1621.

Wang, Y., Wang, Q., Haldar, J. P., Yeh, F. C., Xie, M., Sun, P., ... & Song, S. K. (2011). Quantification of increased cellularity during inflammatory demyelination. *Brain*, *134*(12), 3590-3601.

Wang, X., Cusick, M. F., Wang, Y., Sun, P., Libbey, J. E., Trinkaus, K., ... & Song, S. K. (2014). Diffusion basis spectrum imaging detects and distinguishes coexisting subclinical inflammation, demyelination and axonal injury in experimental autoimmune encephalomyelitis mice. *NMR in Biomedicine*, *27*(7), 843-852.

Wang, Y., Sun, P., Wang, Q., Trinkaus, K., Schmidt, R. E., Naismith, R. T., ... & Song, S. K. (2015). Differentiation and quantification of inflammation, demyelination and axon injury or loss in multiple sclerosis. *Brain*, *138*(5), 1223-1238.

Wang, S., Peterson, D. J., Wang, Y., Wang, Q., Grabowski, T. J., Li, W., & Madhyastha, T. M. (2017). Empirical comparison of diffusion kurtosis imaging and diffusion basis spectrum imaging using the same acquisition in healthy young adults. *Frontiers in neurology*, *8*, 118.

Wang, Q., Wang, Y., Liu, J., Sutphen, C. L., Cruchaga, C., Blazey, T., ... & Benzinger, T. L. (2019a). Quantification of white matter cellularity and damage in preclinical and early symptomatic Alzheimer's disease. *NeuroImage: Clinical*, *22*, 101767.

Wang, Q., Pérez-Carrillo, G. J. G., Ponisio, M. R., LaMontagne, P., Dahiya, S., Marcus, D. S., ... & Wang, Y. (2019b). Heterogeneity Diffusion Imaging of gliomas: Initial experience and validation. *PloS one*, *14*(11), e0225093.

Wilde, E. A., Li, X., Hunter, J. V., Narayana, P. A., Hasan, K., Biekman, B., ... & Levin, H. S. (2016). Loss of consciousness is related to white matter injury in mild traumatic brain injury. *Journal of neurotrauma*, *33*(22), 2000-2010.

Veeramuthu, V., Hariri, F., Narayanan, V., Tan, L. K., Ramli, N., & Ganesan, D. (2016). Microstructural change and cognitive alteration in maxillofacial trauma and mild traumatic brain injury: A diffusion tensor imaging study. *Journal of Oral and Maxillofacial Surgery*, *74*(6), 1197-e1.

Yendiki, A., Panneck, P., Srinivasan, P., Stevens, A., Zöllei, L., Augustinack, J., ... & Fischl, B. (2011). Automated probabilistic reconstruction of white-matter pathways in health and disease using an atlas of the underlying anatomy. *Frontiers in neuroinformatics*, *5*, 23.

Zhang, Y., Brady, M., & Smith, S. (2001). Segmentation of brain MR images through a hidden Markov random field model and the expectation-maximization algorithm. *IEEE transactions on medical imaging*, *20*(1), 45-57.

Zhang, L., Zhang, Y., Li, L., Li, Z., Li, W., Ma, N., ... & Lu, G. (2011). Different white matter abnormalities between the first-episode, treatment-naive patients with posttraumatic stress disorder and generalized anxiety disorder without comorbid conditions. *Journal of affective disorders*, *133*(1-2), 294-299.